



Ice Complex formation in arctic East Siberia during the MIS3 Interstadial



Sebastian Wetterich^{a,*}, Vladimir Tumskoy^b, Natalia Rudaya^c, Andrei A. Andreev^d, Thomas Opel^a, Hanno Meyer^a, Lutz Schirrmeyer^a, Matthias Hüls^e

^a Alfred Wegener Institute, Helmholtz Center for Polar and Marine Research, Research Unit Potsdam, Department of Periglacial Research, Telegrafenberg A43, 14473 Potsdam, Germany

^b Moscow State University, Faculty of Geology, Department of Geocryology, Vorob'evy Gory, 119899 Moscow, Russia

^c Institute of Archaeology and Ethnography, SB RAS, Ak. Lavrentieva 17, 630090 Novosibirsk, Russia

^d University of Cologne, Institute of Geology and Mineralogy, Zùlpicher Str. 49a, 50674 Cologne, Germany

^e Christian-Albrechts-Universität zu Kiel, Leibniz-Laboratory for Radiometric Dating and Isotope Research, Kiel, Germany

ARTICLE INFO

Article history:

Received 27 September 2013

Received in revised form

12 November 2013

Accepted 12 November 2013

Available online

Keywords:

Permafrost

Yedoma

West Beringia

Bol'shoy Lyakhovsky Island

ABSTRACT

A continuous 15 m long sequence of Ice Complex permafrost (Yedoma) exposed in a thermo-cirque at the southern coast of Bol'shoy Lyakhovsky Island (New Siberian Archipelago, Dmitry Laptev Strait) was studied to reconstruct past landscape and environmental dynamics. The sequence accumulated during the Marine Isotope Stage 3 (MIS3) Interstadial between >49 and 29 ka BP in an ice-wedge polygon. The frozen deposits were cryolithologically described and sampled on a vertical bluff between two ice wedges. According to sedimentological and geochronological data, the section is subdivided into three units which correlate with environmental conditions of the early, middle, and late MIS3 period. Paly-nological data support this stratification. The stable isotope signature of texture ice in the polygon structure reflects fractionation due to local freeze–thaw processes, while the signature of an approximately 5 m wide and more than 17 m high ice wedge fits very well into the regional stable-water isotope record. Regional climate dynamics during the MIS3 Interstadial and local landscape conditions of the polygonal patterned ground controlled the Ice Complex formation. The sequence presented here completes previously published MIS3 permafrost records in Northeast Siberia. Late Quaternary stadial-interstadial climate variability in arctic West Beringia is preserved at millennial resolution in the Ice Complex. A MIS3 climate optimum was revealed between 48 and 38 ka BP from the Ice Complex on Bol'shoy Lyakhovsky Island.

© 2013 Elsevier Ltd. All rights reserved.

1. Introduction

Large areas of the modern terrestrial Arctic are underlain by ice-rich permafrost that contains various types of ground ice. Polygonal patterned ground, one of the most common arctic periglacial surface features, is a manifestation of wintertime frost cracking by thermal ground contraction. Ice-filled frost cracks form underground ice wedges whose cracks are repeatedly filled by snowmelt in springtime. The water freezes in the cracks and forms vertical ice veins (Leffingwell, 1915; Lachenbruch, 1962). Iterative frost cracking and ice-vein formation enable ice wedges to grow in height and width, concurrently with sedimentation (syngenetically). Accordingly, the surface above the wedges is shaped into a

polygonal pattern that is marked by polygon rims above the ice wedges when low-centred polygons form (Fig. 1).

Modern polygon tundra landscapes occur abundantly in the arctic coastal plains of Alaska (e.g. Hobbies, 1980), Canada (e.g. Kerfoot, 1972; Young and Abnizova, 2011; Fritz et al., 2012), and Northeast Siberia (e.g. Romanovskii, 1977; Wetterich et al., 2008a). Polygon tundra wetlands in the Arctic have rarely been mapped, although Minke et al. (2007) reported a rough circum-arctic estimate of 250,000 km². Past polygon formation during the Last Glacial period can be deduced from Ice Complex deposits of the Yedoma type (Sher, 1997). Ice Complex formations are widely distributed in arctic lowlands where they have accumulated across the Beringia landmass, and constitute sequences of frozen fine-grained organic-rich polygon fillings up to several tens of meters thick, intersected by syngenetic ice wedges. The area where Ice Complex deposits were commonly distributed in East Siberian lowlands and large river valleys amounts to more than 1,000,000,000 km² (Romanovskii,

* Corresponding author. Tel.: +49 331 288 2207; fax: +49 331 288 2188.
E-mail address: sebastian.wetterich@awi.de (S. Wetterich).

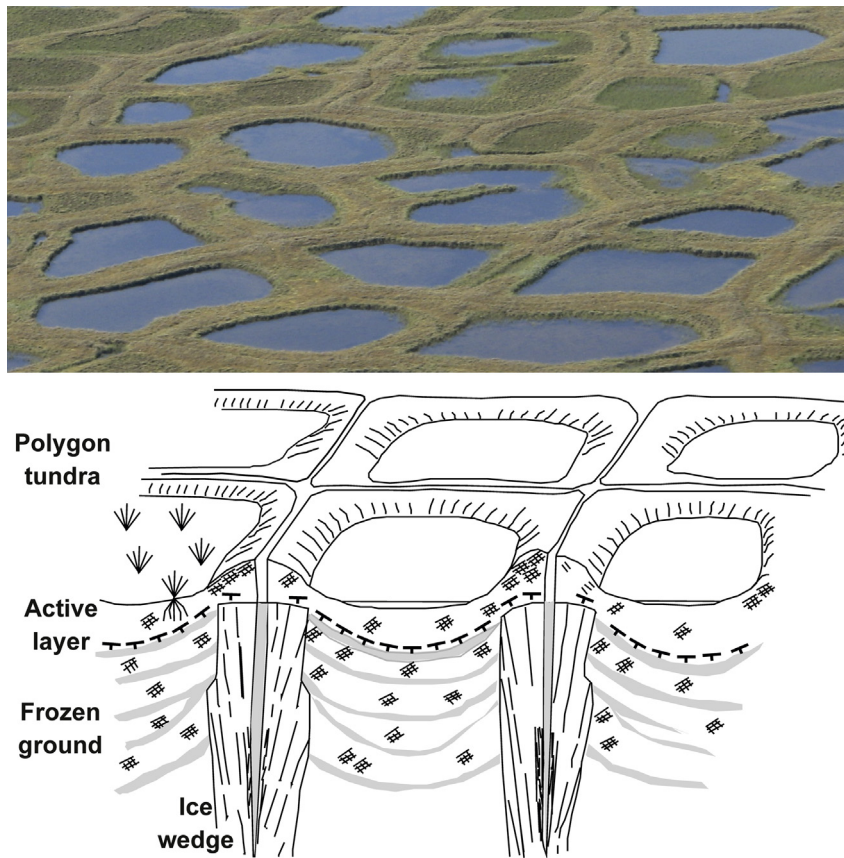


Fig. 1. Schematic cross section (modified after Romanovskii, 1977) and photograph of modern polygonal patterned tundra with low-centered polygon ponds in the Lena Delta. Photograph by K. Piel (formerly AWI Potsdam).

1993; Grosse et al., 2013). Furthermore, Ice Complex formations likely covered the exposed arctic shelves during the Last Glacial period at global sea level low stand (Romanovskii et al., 2004).

Several hypotheses have been suggested to explain the origin of Ice Complex formations (for overview see Schirrmeister et al., 2011a; Schirrmeister et al., 2013). Sher (1997) proposed a poly-genetic origin in which Ice Complex deposits accumulated under different sedimentation regimes, but were largely controlled by similar landscape and relief characteristics, climate conditions, and periglacial processes. An overarching similarity is the presence of large syngenetic ice wedges, and remains of the late Pleistocene mammoth fauna (Nikolskiy et al., 2011) and cold-arid tundra-steppe vegetation (e.g. Blinnikov et al., 2011). An Ice Complex often includes buried peaty cryosols affected by cryoturbation (Gubin, 1994). Poorly-sorted silt and fine-grained sand constitute its clastic part; sometimes coarser-grained sand and gravel are included. Resulting multi-mode grain-size distributions suggest a variety of transport processes, and underscore the importance of joint deposition of silts and coarser grained material (Schirrmeister et al., 2011a).

The frozen sediments contain large amounts of texture ice, i.e. as excess ice. Thin horizontal ice lenses or net-like reticulated ice veins subdivided by ice bands are common. They indicate ice enrichment near the permafrost table under subaerial or shallow subaquatic (i.e. in low-centred polygon ponds) conditions by a slowly aggrading ground surface, changing active-layer thickness, and freezing under poorly-drained conditions. Cryogenic structures in Ice Complex deposits, and in particular the presence of syngenetic ice wedges, are similar at most study sites. Ice wedges often have pronounced shoulders and partial thaw surfaces, indicating

continuous sedimentation but episodic permafrost aggradation with varying active-layer depth on the polygonal ground network (Romanovskii, 1977, 1993).

The development of polygons, including the sedimentation regime and the syngenetic ice-wedge growth, can be described by heterocyclic changes in the active-layer depth leading to a stepwise (not continuous) transformation of seasonally unfrozen into perennially frozen deposits (Vasil'chuk, 2006, 2013). Freezing events that form a new uppermost horizon of perennially frozen ground are reflected by cryogenic horizons. Vasil'chuk (2006, 2013) differentiates the cyclicity of polygon growth into micro-cycles (up to several hundred years), meso-cycles (up to several thousand years), and macro-cycles (up to tens of thousands of years); the latter are controlled by major changes in climate conditions. In contrast, micro- and meso-cycles of polygon growth reflect changes in the sedimentation regime between subaerial and shallow sub-aquatic conditions (Vasil'chuk, 2006).

The East Siberian Ice Complex preserves a diversity of exceptional palaeoenvironmental archives, including ground ice (Meyer et al., 2002; Vasil'chuk et al., 2004; Opel et al., 2011), sediments and cryosols (Gubin and Veremeeva, 2010; Schirrmeister et al., 2011a), faunal (Sher, 1971; Sher et al., 2005; Kiselev and Nazarov, 2009; Nikolskiy et al., 2011) and floral remains (Grichuk and Grichuk, 1960; Giterman, 1985; Kienast et al., 2005; Andreev et al., 2011), ancient DNA (Jørgensen et al., 2012), and a significant, and potentially vulnerable, reservoir of organic carbon (Grosse et al., 2011a,b; Schirrmeister et al., 2011b; Strauss et al., 2012, 2013).

Ice Complex deposits in the East Siberian lowlands and on the New Siberian Islands are of interstadial Marine Isotope Stage 3

(MIS3) age on Kurungnakh Island (3rd terrace of the Lena Delta; Schirrmeister et al., 2003; Wetterich et al., 2008b), on Muostakh Island (Schirrmeister et al., 2011a), at Cape Svyatoi Nos (Nikolskiy and Basilyan, 2004), on the Stol'bovoi and Bel'kovsky islands (New Siberian Archipelago; Schirrmeister et al., 2011a), at the Oyogos Yar coast (Konishchev and Kolesnikov, 1981), in the Yana lowland (e.g. Soplivaya Gora; Basilyan et al., 2009), in the Indigirka lowland (e.g. Allaikha River; Kaplina et al., 1980), and in the Kolyma lowland (e.g. strato type of the Yedomia Suite, Duvanny Yar; Kaplina et al., 1978; Zanina et al., 2011). The stratigraphically most comprehensive coastal outcrop of Ice Complex (MIS4–MIS2) is exposed on Bykovsky Peninsula (Meyer et al., 2002; Schirrmeister et al., 2002a; Slagoda, 2004; Sher et al., 2005).

The study from Bol'shoy Lyakhovsky Island presented here aims at three foci: (1) the description of polygon development during the MIS3 Interstadial in the East Siberian Arctic, and (2) the use of palaeoenvironmental proxy data (sediment, ground ice, pollen) preserved in the studied section in order to (3) deduce interstadial climate, landscape, and vegetation dynamics, the latter in comparison with available regional MIS3 permafrost records.

2. Regional setting

Bol'shoy Lyakhovsky Island is the southernmost island of the New Siberian Archipelago located between the Laptev and the East Siberian seas (Fig. 2). The southern coast of Bol'shoy Lyakhovsky Island exposes permafrost that features frozen sediments, ground ice, and fossil remains dating from the mid-Pleistocene onward (Schirrmeister et al., 2002b; Andreev et al., 2004), and since the late 19th century has been a key area for studying the environmental history of West Beringia (Bunge, 1887; von Toll, 1895; Romanovskii, 1958; Ivanov, 1972; Kunitsky, 1998; Meyer and Dereviagin, 2002; Andreev et al., 2004, 2009; Wetterich et al., 2009, 2011).

The regional Quaternary stratigraphic scheme for the north-eastern part of Siberia was last agreed upon in 1982 and published

in 1987 (Shilo, 1987). Local stratigraphic schemes are distinguished which reflect special features in the geological structure of distinct localities (Shilo, 1987). The main terms and horizons are given in Table 1.

The local stratigraphic scheme for the New Siberian Archipelago and the western part of the Yana-Indigirka lowland is based on geological surveys at a scale of 1:1,000,000 (Ivanov, 1972; Prokhorova and Ivanov, 1973); that was, however, not confirmed by the Inter-institutional Stratigraphic Summit of the Quaternary System of the USSR (Shilo, 1987). A final definition and correlation of Stadials and Interstadials across East Siberia has so far not been agreed upon (Tumskoy and Basilyan, 2009). The on-going discussion about period definitions is evidenced by strata names that vary on regional and local scales and a large deficit in or lack of reliable geochronology (for overview see Shkatova, 2011). A new local stratigraphic scheme for the Dmitry Laptev Strait was proposed by Tumskoy and Basilyan (2006, 2009) and finally published by Tumskoy (2012), including new geochronological data and lithostratigraphical interpretations (Table 1). The geologic structure of deposits exposed at the southern coast of Bol'shoy Lyakhovsky Island is presented in Fig. 3. Following Tumskoy (2012), the latest published work on local stratigraphy, the Yedomia Ice Complex suprahorizon exposed at the southern coast of Bol'shoy Lyakhovsky is subdivided into (1) the Oyogos stadial horizon of the Oyogorskaya Suite (also referred as Zyryan Stadial, MIS4; e.g. Andreev et al., 2009), (2) the Molotkov interstadial horizon of the Oyogorskaya Suite (also referred as Kargin Interstadial; e.g. Anderson and Lozhkin, 2001), and (3) the Sartan stadial horizon of the Yanskaya Suite (MIS2; e.g. Wetterich et al., 2011) (Table 1). The L7-18 Ice Complex exposure presented in this paper refers to the Molotkov (MIS3) interstadial horizon of the Oyogorskaya Suite. It is characterised by ice-rich syncryogenic deposits with huge ice wedges (Fig. 4).

Depending on the prevailing coastal erosion type, Ice Complex outcrops are often exposed in thermo-cirques (thaw slumps) where

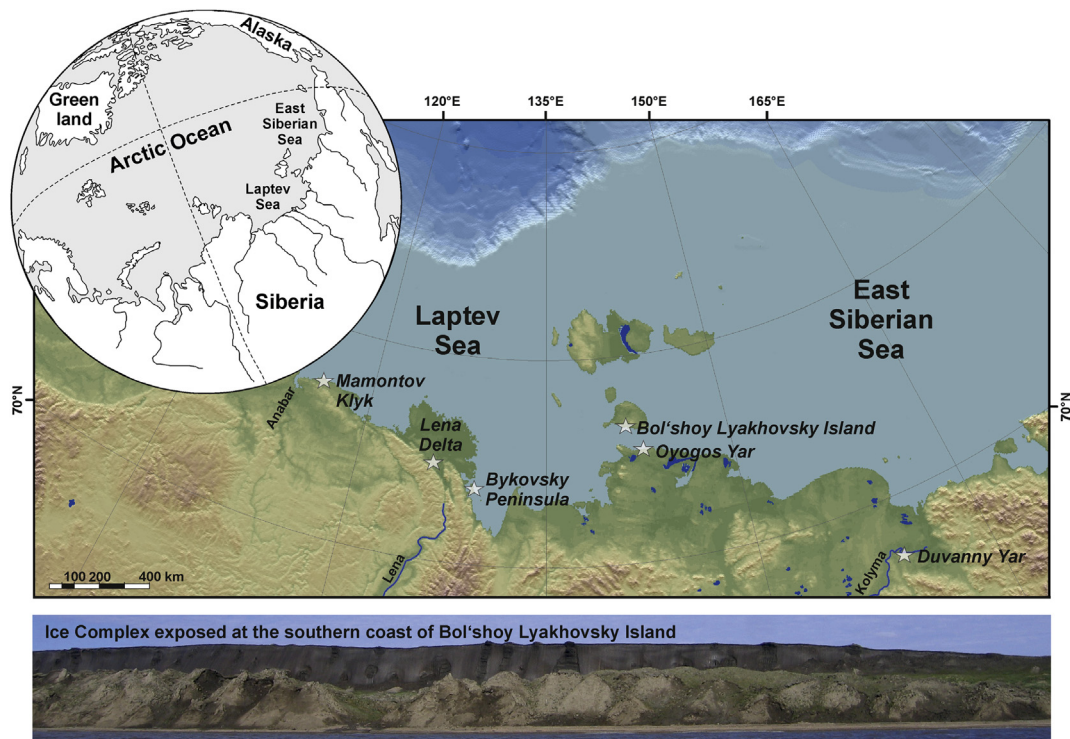


Fig. 2. Map of the study region in the Northeast Siberian lowlands and on the New Siberian Archipelago with various mentioned study sites and the exemplary coastal exposure of the Ice Complex at the southern coast of Bol'shoy Lyakhovsky Island. Map by G. Grosse (UAF).

Table 1
Compilation of stratigraphical units for the Last Glacial period of Yedoma Ice Complex formation (according to ^{*}Tumskoy, 2012; ^{**}Shilo, 1987).

Periods[ka BP]	Local stratigraphy Dmitry Laptev Strait [*]	Regional stratigraphy NE Siberia ^{**}	Period	Corresponding Marine isotope stage
ca 24–10.5	Yedoma suprahorizon	Yanskaya Suite	Stadial	MIS2
ca 57–24		Oyogorskaya Suite	Interstadial	MIS3
ca 71–57			Stadial	MIS4

thermokarst mounds (baydzherakhs) form a thermo-terrace in front of steep walls (Fig. 4). Due to rather intense thermo-denudation (summertime thaw and possible subsequent refreezing of exposed permafrost and material re-deposition) from the upper part of such exposures, radiocarbon-dated sequences could show age inversions caused by re-deposited material. The best available material for stratigraphic and palaeoenvironmental research comes, therefore, from fairly inaccessible steep walls sampled in the frozen state.

The L7-18 exposure was located at the southern coast of Bol'shoy Lyakhovskiy Island, west of the Zimov'e River mouth (73.33512 °N; 141.3300 °E; Fig. 2), and was studied in July 2007 during the joint Russian–German 'Lena – New Siberian Islands' expedition (Schirmer et al., 2008a). The coastal bluff was about 25 m high and was dissected by a thermo-terrace into the uppermost Ice Complex sequence and underlying deposits of the mid-Pleistocene Kuchchugui Suite (Fig. 3).

The studied L7-18 exposure is considered to be representative for late Pleistocene Ice Complex on regional scale because similar structures have been observed along the entire southern coast of Bol'shoy Lyakhovskiy Island as well as along the continental coast of the Dmitry Laptev Strait (Oyogos Yar; Fig. 2).

3. Material and methods

3.1. Fieldwork

Using alpinist's equipment, the cryolithological features of a steep wall of the Ice Complex were studied. Samples were taken every 0.5–1 m in a continuous sequence between two ice wedges (Fig. 4, SOM 1). In total, 23 samples were obtained using axe and hammer, 22 of them sediment samples. One ice sample (L7-18-05)

was taken from an ice band. The gravimetric ice content of the frozen deposits was estimated immediately after thawing by comparing the weight of the frozen sample to the weight of the dry sample, expressed as weight percentage (wt%) (van Everdingen, 1998). Upon return to the laboratory the samples were freeze-dried, carefully manually homogenised, and split into subsamples for sedimentological, geochemical, and palynological analyses.

3.2. Sedimentology and biogeochemistry

Granulometrical analyses were conducted using a laser-particle analyser (Beckmann Coulter LS 200) and computed with GRADISTAT 4.0 software (Blott and Pye, 2001). The mass-specific magnetic susceptibility (MS) was analysed with a Bartington MS2 instrument equipped with a MS2B sensor. The total organic carbon (TOC), total carbon (TC), and total nitrogen (TN) contents were measured with a carbon–nitrogen–sulphur (CNS) analyser (Elementar Vario EL III). The carbon to nitrogen (C/N) ratio was calculated as the TOC/TN ratio. The total inorganic carbon (TIC) content was estimated as the difference between TC and TOC. Stable carbon isotope ratios ($\delta^{13}\text{C}$) in TOC were measured with a Finnigan DELTA S mass spectrometer coupled to an FLASH element analyser and a CFOLIO III gas mix system after removal of carbonates with 10% HCl in Ag-cups and combustion to CO_2 . Accuracy of the measurements was determined by parallel analysis of internal and international standard reference material (CaCO_3 12%; NCSDC 73311[GSD-1], China National Center for Iron and Steel, Beijing, China; Marine Sediment, High Purity Standards, Charleston SC, USA; SOIL, LECO Corporation St. Joseph MI, USA; IVA33802150, IVA99994, IVA99995, IVA99996, IVA Analysetechnik, Meerbusch, Germany). The analyses were accurate to $\pm 0.2\text{‰}$. The $\delta^{13}\text{C}$ values are expressed in delta per mil notation (δ , ‰) relative to the Vienna Pee Dee Belemnite (VPDB) Standard.

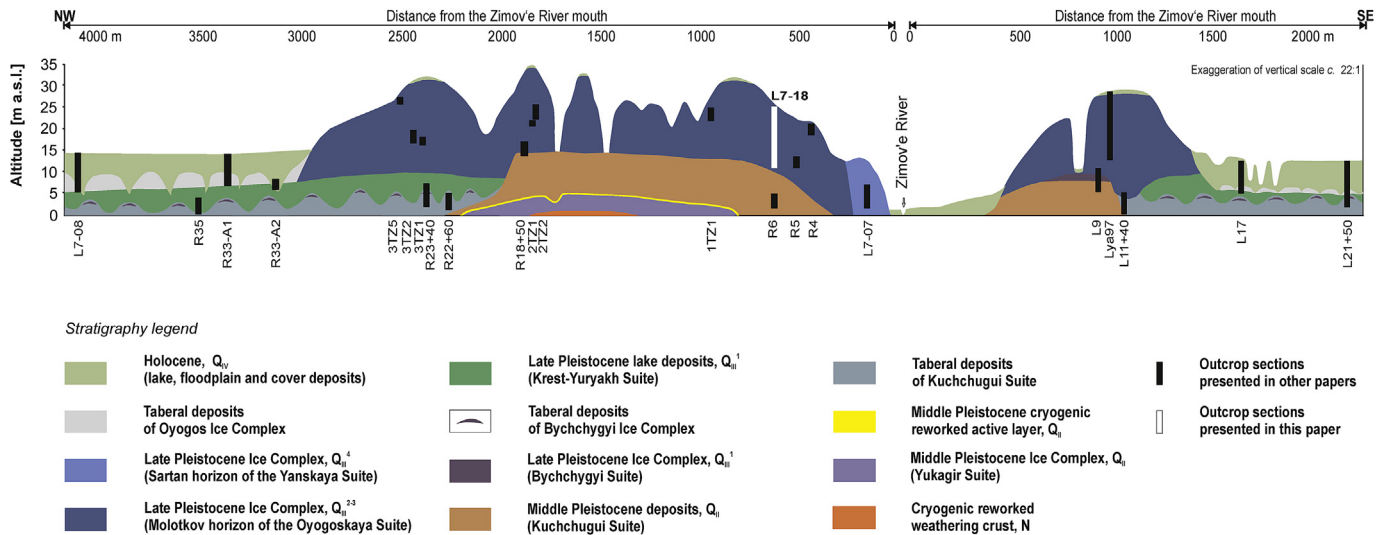


Fig. 3. Stratigraphic scheme of the exposed coastal section at the Zimov'e River mouth on the southern coast of Bol'shoy Lyakhovskiy Island modified after Andreev et al. (2004, 2009) and updated according to Tumskoy (2012). Studied profiles from previous work (Andreev et al., 2004, 2009; Ilyashuk et al., 2006; Wetterich et al., 2009, 2011) are shown by black vertical bars. The position of the L7-18 Molotkov (MIS3) interstadial profile is shown by a white vertical bar.

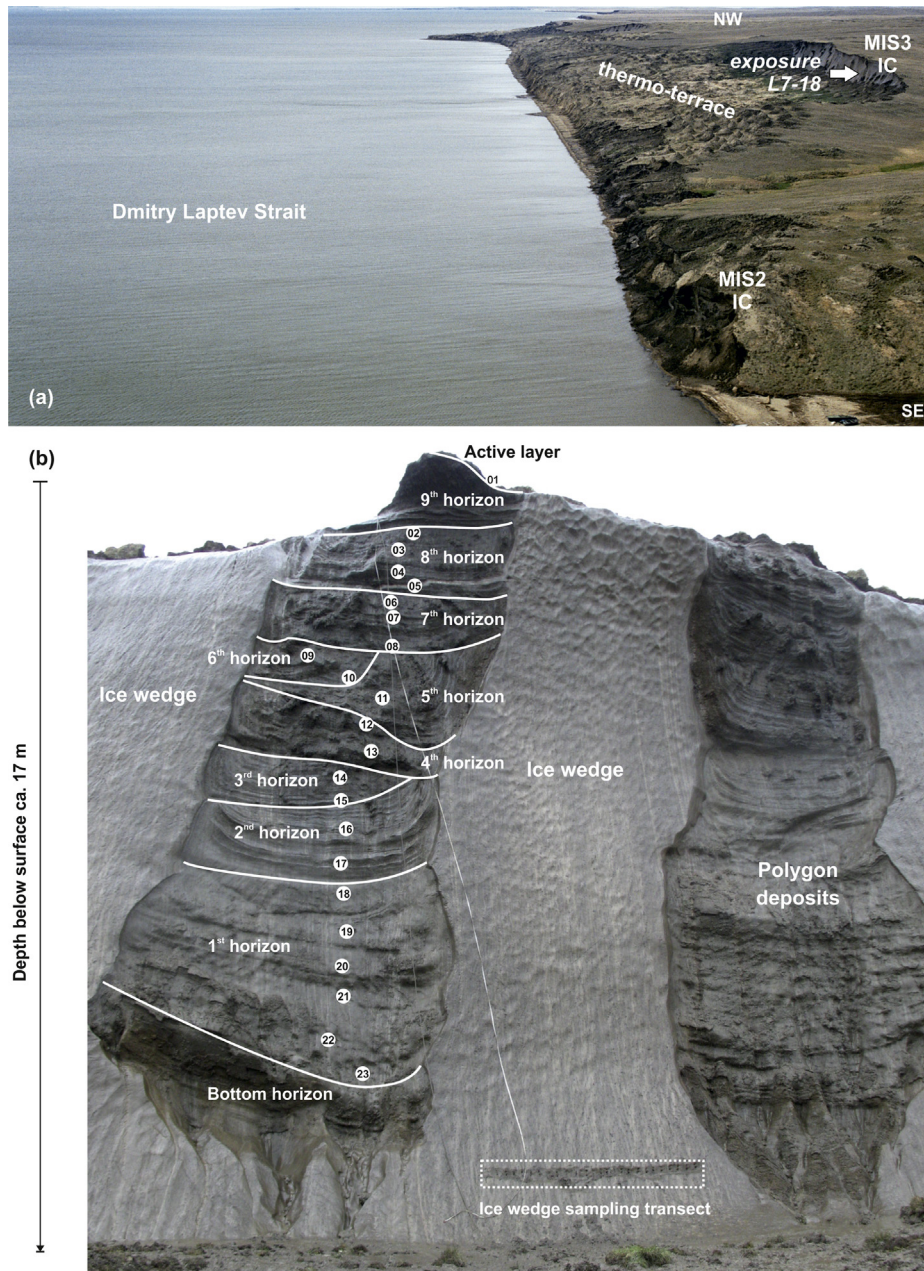


Fig. 4. Exposure situation at the southern coast of Bol'shoy Lyakhovsky Island with (a) proximity of the L7-18 MIS3 Ice Complex (IC) section and the L7-07 MIS2 Ice Complex (IC) section (Wetterich et al., 2011); and (b) photograph of the studied L7-18 section with cryolithological horizons and sample positions.

3.3. Stable water isotopes ($\delta^{18}\text{O}$, δD)

Using ice screws, a total of 25 samples was taken in a 4.5-m-wide horizontal transect across an exposed syngenetic ice wedge about 16 m below the surface (Fig. 4).

Samples from this ice wedge (Fig. 4) were analysed for their stable water isotope composition ($\delta^{18}\text{O}$, δD) which reflects winter air temperature with lighter (more negative values) reflecting colder conditions and heavier (less negative) warmer condition (e.g. Meyer et al., 2002). Equilibration technique was applied using a mass spectrometer (Finnigan MAT Delta-S) with reproducibility derived from long-term standard measurements of 1σ better than $\pm 0.1\text{‰}$ for $\delta^{18}\text{O}$ and $\pm 0.8\text{‰}$ for δD (Meyer et al., 2000). All samples were run at least in duplicate. The values are given as δ , ‰ relative to the Vienna Standard Mean Ocean Water (VSMOW) Standard.

Supernatant water from 17 sediment samples, i.e. from thawed texture ice, was likewise analysed.

3.4. Radiocarbon dating

For 20 samples (4 samples were prepared and measured twice) plant material was isolated for radiocarbon measurements (Table 2) using standard procedures; wet-sieving at $250\ \mu\text{m}$, drying, identification of plant remains under microscope. The radiocarbon dating was conducted using the accelerator mass spectrometry (AMS) facilities at the Leibniz Laboratory for Radiometric Dating and Stable Isotope Research (Kiel, Germany; Grootes et al., 2004). For all selected samples we used well established treatment and measurement protocols (Nadeau et al., 1997, 1998); inspection under microscope to avoid possible contamination introduced during

Table 2
AMS-measured uncalibrated radiocarbon ages in samples of the L7-18 profile from Bol'shoy Lyakhovskiy.

Sample N ^o	Lab no	Material	Measured sample size [mg C]	¹⁴ C corrected [pMC]	δ ¹³ C [‰ VPDB]	Depth [m b.s.]	Radiocarbon ages [¹⁴ C yr BP]	
L7-18-02	KIA49288	Remains of <i>Bryum</i> and liverwort	0.3	30.35 ± 0.59	-28.27 ± 0.15	1.2	9580	+160/-150
L7-18-02	KIA44913	Remains of <i>Drepanocladus</i> , <i>Rumex acetocella</i> s.l., <i>Cerastium</i> , Poales	0.8	2.59 ± 0.21	-26.63 ± 0.09	1.2	29,350	+680/-630
L7-18-04	KIA49289	Remains of <i>Drepanocladus</i>	1	2.72 ± 0.16	-35.05 ± 0.46	2.5	28,970	+500/-470
L7-18-04	KIA44914	Remains of <i>Drepanocladus</i>	1.03	2.42 ± 0.12	-30.78 ± 0.11	2.5	29,890	+390/-380
L7-18-07	KIA49290	Stems of mosses, seeds of Caryophyllaceae, <i>Carex</i> , <i>Rumex acetocella</i> s.l., <i>Potentilla</i> cf. <i>arenosa</i> , <i>Ranunculus affinis</i> , <i>Cerastium</i> , <i>Stellaria longipes</i> , <i>Minnartia rubella</i>	0.2	1.15 ± 0.65	-26.57 ± 0.21	3.3	>29,780	
L7-18-08	KIA44915	Stems of mosses, seeds of <i>Carex</i>	1.4	1.51 ± 0.12	-26.67 ± 0.18	4.1	33 680	+670/-620
L7-18-09	KIA44916	Stems of mosses, seeds of <i>Carex</i> undefined wood and root remains	3.4	0.84 ± 0.06	-28.68 ± 0.20	4.6	38 410	+580/-540
L7-18-10	KIA49291	Undefined leaf and wood remains	1.82	0.74 ± 0.09	-28.10 ± 0.12	4.85	39 390	+1090/-960
L7-18-11	KIA44917	Undefined root remains	1.3	0.74 ± 0.13	-27.49 ± 0.10	5.4	39 450	+1510/-1270
L7-18-12	KIA49292	Stems of mosses, seeds of <i>Carex</i> , <i>Rumex acetocella</i> s.l., <i>Ranunculus affinis</i> , undefined wood remains	1.6	0.31 ± 0.10	-25.28 ± 0.32	6	46 320	+3190/-2280
L7-18-13	KIA44918	Leaf and seed remains of <i>Carex</i>	2.1	0.44 ± 0.08	-28.71 ± 0.11	6.6	43 550	+1640/-1360
L7-18-14	KIA49293	Undefined wood remains	2.3	0.12 ± 0.08	-28.15 ± 0.18	7.2	>47 360	
L7-18-15	KIA44919	Leaf and seed remains of <i>Carex</i> , undefined wood remains	3.5	0.24 ± 0.05	-27.48 ± 0.12	7.7	48 570	+2060/-1640
L7-18-16	KIA44920	Undefined plant remains	1.4	0.05 ± 0.11	-28.64 ± 0.11	8.4	>47140	
L7-18-16	KIA49294	Undefined plant remains	1.5	0.25 ± 0.11	-25.54 ± 0.17	8.4	48 240	+4900/-3020
L7-18-17	KIA49295	Undefined plant remains	0.8	0.14 ± 0.21	-25.90 ± 0.09	9.1	>41630	
L7-18-18	KIA44921	Undefined plant remains	3.3	0.12 ± 0.06	-28.10 ± 0.12	9.65	53 770	+4750/-2970
L7-18-18 ^a	KIA44921	Undefined plant remains				9.65	>49814	
L7-18-20	KIA49296	Undefined plant remains	3.4	0.47 ± 0.06	-26.37 ± 0.11	11.1	43 010	+1020/-910
L7-18-20	KIA49297	Remains of <i>Potentilla</i> , <i>Cerastium</i> and Caryophyllaceae	0.8	0.00 ± 0.20	-26.42 ± 0.18	11.1	>44390	
L7-18-22	KIA44922	Remains of <i>Cerastium</i> and <i>Carex</i> , few moss remains	1	0.32 ± 0.16	-27.95 ± 0.15	12.5	46 150	+5400/-3200

^a See detailed discussion of sample KIA44921 in chapter 5.1.

sieving and drying; extraction with 1% HCl, 1% NaOH at 60 °C and again 1% HCl (AAA treatment, acid-alkali-acid) to remove adhering carbonate and organic contamination such as fulvic and humic acids (alkali residue); after drying, an appropriate amount of sample material was converted to CO₂ during combustion at 900 °C of sample material which was flame-sealed in a quartz tube together with CuO and silver wool; graphitisation of sample CO₂ with H₂ over Fe powder as catalyst. Resulting carbon/iron mixture was pressed into a pellet in an aluminium target holder for AMS measurements. The ¹⁴C concentration of the samples was measured with a 3 MV HV Tandemron accelerator mass spectrometer (AMS). Simultaneously collected ¹⁴C, ¹³C, and ¹²C beams of each sample were compared with those of Oxalic Acid standard CO₂ (modern standard) and background material (fossil organics containing no ¹⁴C such as North-Sea crude-oil and Anthracite). Conventional ¹⁴C ages were calculated according to Stuiver and Polach (1977) with a δ¹³C correction for isotopic fractionation based on the ¹³C/¹²C ratio measured by our AMS-system simultaneously with the ¹⁴C/¹²C ratio. This δ¹³C includes the effects of fractionation during graphitisation and in the AMS-system and, therefore, cannot be compared with δ¹³C values obtained per mass spectrometer on CO₂. For the determination of our measuring uncertainty (standard deviation, σ) we observed both the counting statistics of the ¹⁴C measurement and the variability of the interval results that, together, made up one measurement. The larger of the two was adopted as measuring uncertainty. To this we added the uncertainty connected with the subtraction of our 'blank'. The quoted 1σ uncertainty was thus our best estimate for the full measurement and not just based on counting statistics. For old samples, e.g. samples containing a low amount of ¹⁴C, background effects basically determine the detection limit for radiocarbon measurements.

To correct for detected ¹⁴C isotopes which are artefacts caused by machine background (e.g. ¹⁴C ions are detected in a ¹⁴C free target) and/or ¹⁴C introduced during sample treatment (chemistry, CO₂ conversion and graphitisation), fossil samples which should not contain detectable amounts of ¹⁴C were measured. Here, results of the background measurements of fossil anthracite, treated similar to the unknown samples, were subtracted. For measurements which gave zero or negative ¹⁴C concentrations after the correction (including measurement uncertainties), a minimum age was calculated using two times the measurement uncertainties. All radiocarbon dates throughout this paper are reported as uncalibrated ages in ka BP.

3.5. Palynology

A total of 22 samples, each consisting of two grams of dry sediment, were treated for pollen analysis using the standard procedure included treatment with HCl and KOH, sieving (250 μm), treatment with HF, acetolysis, and mounting in glycerin (Fægri and Iversen, 1989). Two *Lycopodium* spore tablets were added to each sample in order to calculate total pollen and spore concentrations (Stockmarr, 1971). Pollen and spore residues mounted in glycerin were analysed under a light microscope Zeiss Axiolmager D2 at 400× magnification. Identification of the pollen and spores was performed using a reference pollen collection and pollen atlases (Kuprianova and Alyoshina, 1972; Beug, 2004). Non-pollen palynomorphs (NPPs) were identified using descriptions, pictures and photographs published by Jankovska (1991) and van Geel (2001). In total, 45 pollen and spore taxa were identified. The microscopic analysis revealed moderately high pollen concentration and generally good preservation of pollen grains allowing easy counting

of up to 300 terrestrial pollen grains per sample. Percentages of all taxa were calculated based on setting the total of all pollen and spore taxa equal to 100%. Results of pollen analysis are displayed in the pollen diagram produced with the Tilia/TiliaGraph software (Grimm, 1991, 2004). In the diagram, visual definition of the pollen zones (PZs) is supported by CONISS software.

4. Results

4.1. Geochronology

The chronology of the L7-18 exposure is based on 20 radiocarbon-dated sediment samples. Radiocarbon concentrations varied between 0.12 percent modern carbon (pMC) and 30.35 pMC, equivalent to calculated radiocarbon ages of 53,770 yr BP and 9580 yr BP. Corrected radiocarbon concentrations and ages are summarised in Table 2. Generally, the sequence between 10 and 1 m b.s. shows a decrease in sample ages from about 53 ka BP to about 29 ka BP (Fig. 5). However, the chronology is complicated by age determinations which gave minimum (infinite) ages, and dates which are interpreted as age inversions due to re-deposition. Both, the infinite and the redeposited dates do not contribute to further palaeoenvironmental interpretation although they mirror the overall accumulation period of the studied sequence. A depth-age relation was deduced using 12 radiocarbon-dated samples with finite ages (Fig. 5). Here, the 95% confidence band is given to illustrate the depth-age correlation ($r^2 = 0.95$) of the interval between about 53 and 29 ka BP. To the sample L7-18-18 that contained the oldest date of the sequence (53,770 ka BP) a background correction using fossil plant material was applied leading to an infinite age of >49,814 yr BP. Therefore, the interval between >49 and 29 ka BP is used in further geochronological interpretation of the data. The measured radiocarbon ages and the observed age inhomogeneities of the L7-18 Ice Complex sequence are discussed in detail in chapter 5.1.

4.2. Cryolithological description

During field description the sequence was subdivided into 11 horizons, which vary in colour, cryostructures, and sediment composition (Fig. 4, SOM 1). The ground ice including texture ice and ice-wedge ice was of special interest at exposure L7-18. Two large ice wedges at least 17 m in vertical extension and 3–5 m in width border the sampled section. At the lateral contact between the frozen sediment columns and the ice wedges, 'ice-wedge shoulders' are visible which reflect the interaction between the growing ice wedge and the intrapolygon sediments as well as the active-layer depth during syn-cryogenic Ice Complex formation. According to cryolithological features, the L7-18 sequence was separated into 9 cryogenic horizons (or cycles; Vasil'chuk, 2006) that correspond to certain stages in polygon development during sedimentation. The lowermost exposed horizon is named the bottom layer. The 1st cryogenic horizon shows massive and microlens-like cryostructures. Starting with the 2nd cryogenic horizon, banded and net-like (lens-like reticulated) cryostructures occur. Banded ice structures represent a past maximum active-layer position from which soil moisture migrated towards the frozen underground, segregated, and froze at the border between the permafrost and the active layer. Such banded ice occurs within a cryogenic horizon at different depths. Towards the margin of the neighbouring ice wedge, ice bands and adjacent sediments are bent upwards and point to distinct ice wedge shoulders. Such shoulders resemble a cryogenic horizon because they form due to changes in the sedimentation regime and corresponding growth of the neighboring syngenetic ice wedges (e.g. Popov, 1978). Between ice

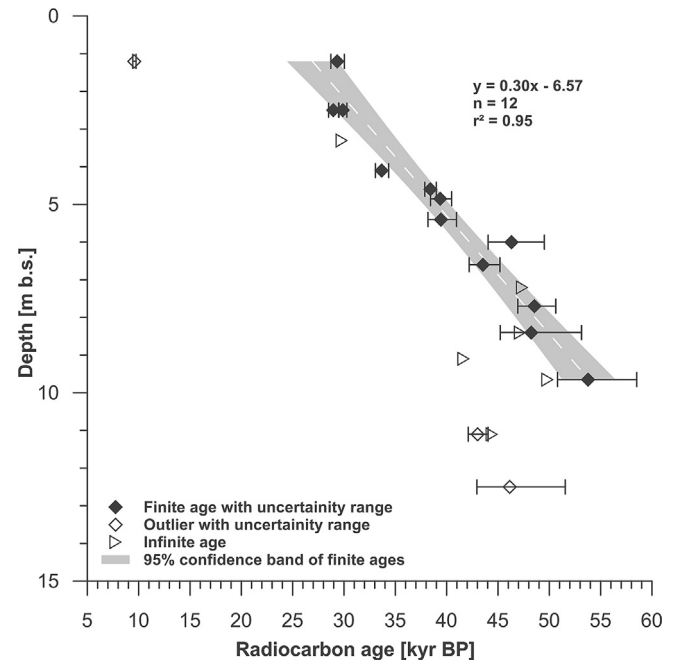


Fig. 5. Bi-plot of sample depth below surface and radiocarbon age of the L7-18 the Molotkov (MIS3) interstadial section. The 95% confidence band for 12 finite ages is shown in grey.

bands, net-like ice structures occur that formed via repeated freezing and thawing within the seasonally unfrozen surface (active) layer. Such structures are indicative of pore water (pore ice) supersaturation. The uppermost horizon includes the thawed modern active layer.

4.3. Sediment and ground-ice records

According to its sedimentary inventory the sequence is divided into three main sediment units (unit A to C; Fig. 6). The bottom layer between 14.3 and 13.3 m b.s. was not sampled.

Sediment unit A (13.3–8 m b.s., >49–48 ka BP) is composed of the 1st and 2nd cryogenic horizons (Fig. 6). The differentiation between the horizons is evidenced by ice structures which are microlens-like in the 1st, and banded in the 2nd cryogenic horizon. The sediments are poorly-sorted fine-grained sands or coarse-grained silts which are rather unimodally distributed (Fig. 7). The MS reaches maximum values of around $40 \cdot 10^{-8} \text{ m}^3 \text{ kg}^{-1}$. The TOC is low (<1.5 wt%). The $\delta^{13}\text{C}$ of TOC values are -25‰ and heavier while the C/N values are low, between about 7.8 and 9.2. The gravimetric ice content is as low as 43–56 wt% in the 1st cryogenic horizon and reaches values as high as 140 wt% in the 2nd cryogenic horizon. The $\delta^{18}\text{O}$ and δD values of the texture ice increase upward from about -34 to -25.7‰ and from about -247 to -200‰ , respectively. The d excess decreases from about 28 to 5‰ (Fig. 8).

The rather unimodal distribution of the coarse-grained silt (Fig. 7) characterises deposits of sediment unit B that include the 3rd–5th cryogenic horizons (8–5 m b.s., 48–39 ka BP; Fig. 6). A distinct decrease in MS from 30 to $15.5 \cdot 10^{-8} \text{ m}^3 \text{ kg}^{-1}$ indicates changing magnetic properties and/or sediment sources. Increased TOC (up to about 6.3 wt%) reflects higher peat content and might explain the decreasing MS. Total inorganic carbon (TIC) reflecting carbonate content is as high as 0.7 wt%. The $\delta^{13}\text{C}$ of TOC values are lighter than in unit A (Fig. 6), pointing to a different source (vegetation) for the organic matter; the higher C/N (above 9.3) indicates less decomposition of organic matter, likely due to moister (more

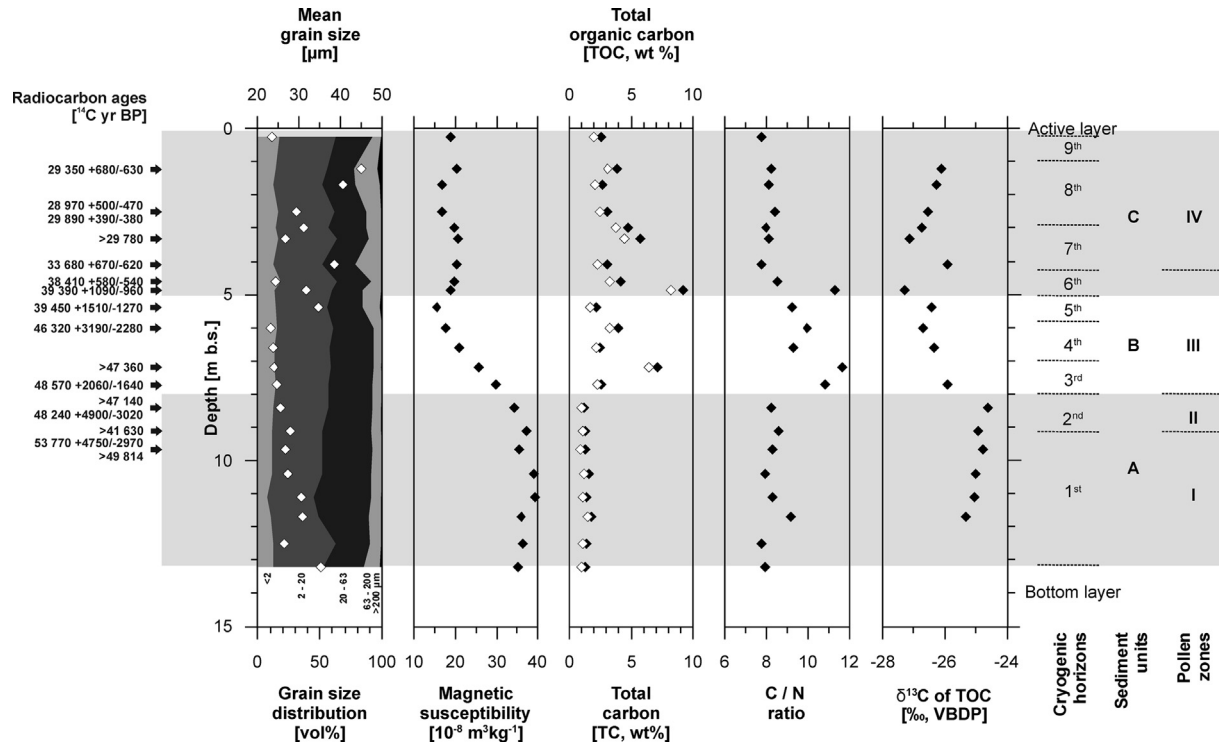


Fig. 6. Cryolithological, sedimentological, and geochronological data from the L7-18 Molotkov (MIS3) interstadial profile. Note that data labelled on the lower x axes are shown by black diamonds and data labelled on the upper x axes (i.e. mean grain size, TOC values) are shown by open diamonds. The profile zonation according to cryogenic horizons, pollen zones, and sediment units is given at the right-hand side for comparison. Sediment units are highlighted by grey areas.

anaerobic) conditions existing in the active layer between deposition and permanent freezing of the deposits. The stable water isotope signature of texture ice is relatively stable and averages about -27.5‰ in $\delta^{18}\text{O}$, -214‰ in δD , and 6.9‰ in d excess (Fig. 8).

Sediment unit C (5–0.35 m b.s., 39–29 ka BP) comprises the 6th–8th cryogenic horizons, and the uppermost modern active layer (Fig. 6). The 9th cryogenic horizon was not sampled. The trimodal grain size distribution of the poorly sorted coarse or sandy silts (Fig. 7) points to underlying units that were laid down in different depositional milieus. The MS remains low, around $20 \cdot 10^{-8} \text{ m}^3 \text{ kg}^{-1}$. The organic carbon content is variable (TOC between about 2 and 8 wt%); higher values represent peaty layers with enriched organic matter content. TIC reaches 1.3 wt% and might be related to carbonate shells of freshwater organisms (ostracods, mollusks) that inhabited the small ponds of low-center polygons. The $\delta^{13}\text{C}$ of TOC of around -26.5‰ is somewhat lighter than in the underlying units A and B. Except for the lowermost sample of unit C, the C/N ratio is around 8.1. The gravimetric ice content reaches 173 wt%. Texture ice stable water isotopes do not differ from values of the underlying unit B with averages of about -27.7‰ in $\delta^{18}\text{O}$ and -219‰ in δD . d excess of 3.1‰ is lower than in unit B (Fig. 8).

The overall image of L7-18 profile sediment properties from unit A to C is characterised by increasing grain size within the silt fraction, by a change from a rather unimodal to a polymodal distribution pattern, and by gradually decreasing MS (Fig. 6). Comparing the biogeochemical parameters, unit A is characterised by low TOC, and TIC, low C/N, and heavier $\delta^{13}\text{C}$ of TOC while units B and C show increased carbon contents, lower decomposition state of organic matter, and a lighter $\delta^{13}\text{C}$ of TOC.

The ice-wedge profile samples (Fig. 4) show depleted values in a narrow range of -31.9 to -30.3‰ (mean -31‰) in $\delta^{18}\text{O}$ and -251 to -238‰ (mean -243‰) in δD , pointing to relatively stable, cold

winter conditions during ice-wedge formation (Fig. 9). The d excess values vary between 3.9 and 7.8‰ (mean 5.4‰) and plot well below the Global Meteoric Water Line (GMWL; Craig, 1961). The regression in a $\delta^{18}\text{O} - \delta\text{D}$ co-isotope plot (Fig. 9) exhibits a slope of 8.9 ($n = 25$), somewhat above that of the GMWL (slope of 8). The texture-ice data slope of 5.2 ($n = 17$) is distinctly lower than that for ground ice from meteoric sources (i.e. ice wedges) and indicates significant secondary fractionation during texture-ice formation.

4.4. Pollen records

The pollen diagram is subdivided into four PZs based on changing pollen taxa composition and abundances (Fig. 10). Non-pollen palynomorphs (NPPs) are represented by algae (*Zygnema*, *Botryococcus*), fungal (*Glomus*, *Microthyrium*), and Tardigrada (*Macrobiotus*) remains.

PZ I (13.3–9.2 m b.s., >49 ka BP) is characterised by low pollen concentration and dominance of herbaceous taxa (up to 80%) including Poaceae (up to 40%), Cyperaceae (up to 20%), Ranunculaceae, and Papaveraceae. Contents of arboreal taxa are the highest in this profile (up to 40%); however, coniferous pollen appears to have been reworked. Most of the Pinaceae pollen grains have more dark colours, different autofluorescence and raptures of exine.

PZ II (9.2–8 m b.s., 49–48 ka BP) is characterised by the dominance of Poaceae pollen (up to 60%) among herbaceous taxa. Cyperaceae, Ranunculaceae, and Papaveraceae pollen are also relatively abundant. Contents of *Artemisia* pollen are higher as compared with other PZs. The percentage of arboreal pollen decreases but is still relatively high (up to 15%).

PZ III (8–4.2 m b.s., 48–38 ka BP) is notable for an increase in total pollen concentration accompanied by a decrease of arboreal pollen abundance. However, the content of *Salix* pollen is significant in PZ III (up to 4%). Among herbs, Cyperaceae pollen dominates

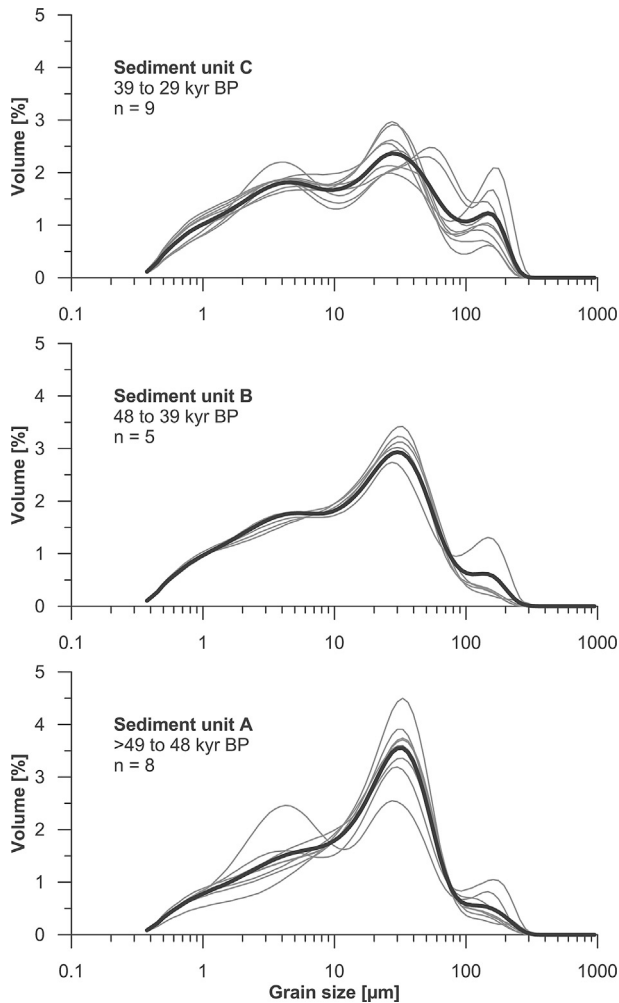


Fig. 7. Grain size distribution curves of the different sediment units of the L7-18 Molotkov (MIS3) interstadial profile. Mean values for each unit are shown by the bold curve.

(up to 70%). Caryophyllaceae is the third most abundant of the herbaceous pollen in this zone. A single pollen grain of *Nuphar* was found in the lower part of PZ III. The abundance of *Zygnema* remains also increases in PZ III.

PZ IV (4.2–0.35 m b.s., 38–29 ka BP) shows evidence of a slight decrease of Cyperaceae pollen and increase of Poaceae pollen abundance. Arboreal pollen is represented by single grains of Pinaceae, *Betula*, *Alnus*, and *Salix*. However, *Salix* pollen occurs constantly through the profile.

5. Discussion

5.1. Chronology of the MIS3 permafrost sequence

The approach of radiocarbon dating to permafrost samples from the MIS3 is complicated by permafrost-related processes like cryoturbation at the deposition time of a certain horizon, and thawing, transport and re-freezing of material. Both processes relocate material and lead to age inversions. Furthermore, the age of the MIS3 deposits itself reaches the limit of the radiocarbon dating method and cause to high uncertainties or infinite ages. Other dating methods are not easily applicable. Ice Complex permafrost samples are not datable so far by Optically-Stimulated Luminescence (OSL) due to their variable and partly very high ice content that

attenuates the dose rate of the ambient radiation collected by a sample, and consequently affects the age determination. The isochron uranium–thorium disequilibria ($^{230}\text{Th}/\text{U}$) technique might be an option to date permafrost older than the limit of radiocarbon dating (Wetterich et al., 2008b), but $^{230}\text{Th}/\text{U}$ dating is only appropriate for organic-rich (peat) sediments under the precondition that the peat adsorbed groundwater-dissolved uranium during formation and acted further on as chemically closed system for uranium (e.g. Geyh, 2001). In this context, a chronology of MIS3 Ice Complex based on radiocarbon-dates holds its own difficulties which are discussed below, but is however appropriate.

The measured radiocarbon ages and the observed age inhomogeneities of the studied L7-18 sequence allow a rather rough age model for the upper 10 m, ranging from about 53 ka BP to about 29 ka BP. On a smaller scale, age plateaus and inversions indicate inhomogeneities which could be related to mixing due to cryoturbation or thaw-induced re-deposition of the dated material. For example, the Holocene age in sample KIA 49288 in contrast to KIA 44913 (both dates from L7-18-02) indicates cryoturbation within this horizon. Furthermore, the samples L7-18-12 (KIA 49292) and L7-18-16 (KIA 49294 and KIA 44920) are considered to have undergone cryoturbation, i.e. relocation within the thawed active layer shortly after deposition. Samples below 10 m b.s. show either slightly younger finite radiocarbon ages (L7-18-20, KIA 49296; L7-18-22, KIA 44922) or infinite ages (L7-18-17, KIA 49295; L7-18-20, KIA 49297). The younger ages are likely related to modern erosion processes when thawed younger material from higher positions at the cliff falls down and re-freezes at lower positions. The oldest measured sample in this sequence is sample L7-18-18 (KIA44921; 0.12 ± 0.06 pMC, $53\,770 \pm 4750/-2970$ yr BP). We consider this age as rather tentative. Preliminary results of a study of different background materials, performed by one co-author (M. Hüls, Leibniz-Laboratory for Radiometric Dating and Isotope Research, Kiel, Germany) seem to indicate a dependence between the measured material (e.g. coal, plant remains, bone collagen) and the magnitude of the background correction (Grootes et al., 2011), likewise to what was observed for carbonate material (Nadeau et al., 2001). Different from the background correction applied using fossil coal, plant materials seem to indicate a larger necessary correction which would shift corrected radiocarbon age towards older ages. Applying the still very preliminary results of a plant-based background to the measurement of sample L7-18-18 (KIA44921), the corrected age would become infinite, around $>49\,814$ yr BP. All measured ages for the sequence reported here would experience an age shift, which, however, would not be statistically significant considering the measured uncertainties. Alas, the study regarding different background materials has not reached an acceptable stage to be applied reliably, and needs thorough verification. Nevertheless, it is mentioned here to raise the awareness in general for age uncertainties for radiocarbon dates in this time range with remaining radiocarbon concentrations <1 pMC.

For the samples L7-18-07 (KIA49290), L7-18-14 (KIA49293), L7-18-16 (KIA44920), L7-18-17 (KIA49295), and L7-18-20 (KIA49297) (Table 2) with zero or negative ^{14}C concentrations after the correction, a minimum age is calculated using two times the measurement uncertainties. The infinite minimum age of sample L7-18-07 (KIA49290) is caused by a very small sample size (carbon amount measured: 200 μg) due to a larger background correction necessary for smaller samples. The district position of the studied L7-18 sequence between two ice wedges which do not exhibit thaw unconformities however support our assumption of continuous deposition of the Ice Complex material. Considering the dating difficulties mentioned above the accumulation period of the L7-18 Ice Complex is assumed between about >49 ka BP and 29 ka BP.

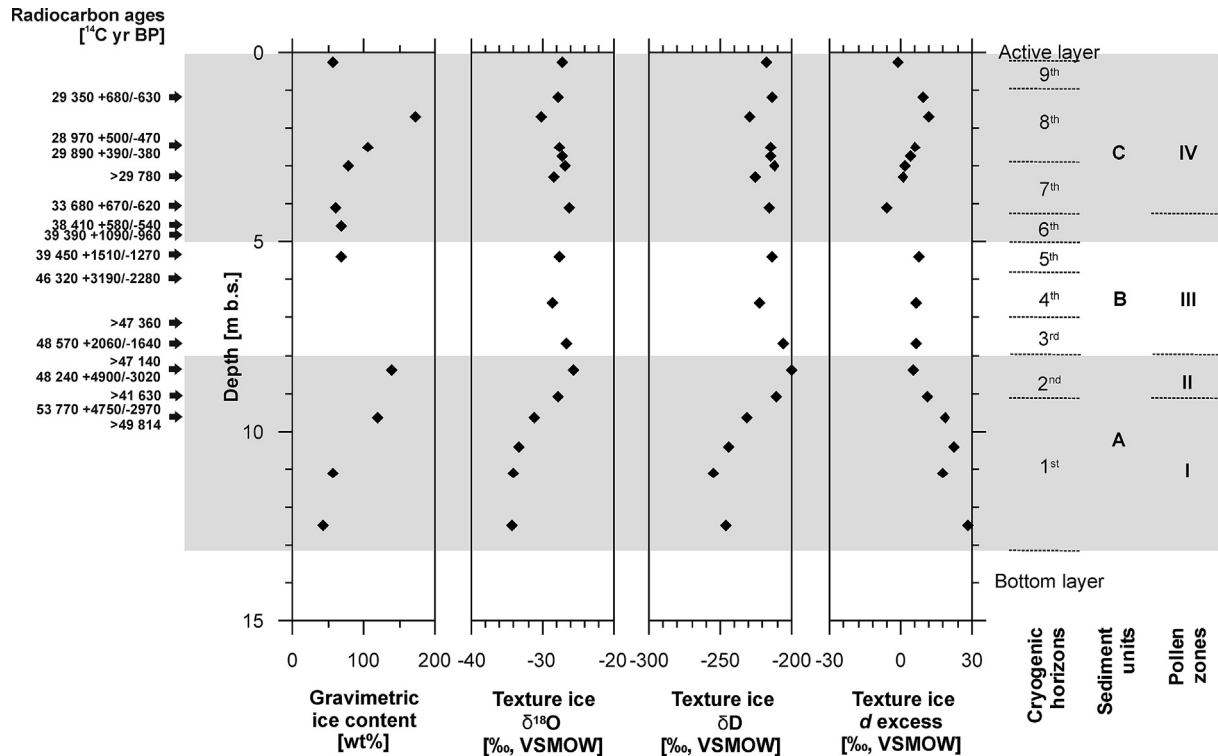


Fig. 8. Gravimetric content of texture ice in sediment samples, and stable texture ice water isotope composition from the L7-18 Molotkov (MIS3) interstadial profile. The profile zonation according to cryogenic horizons, pollen zones, and sediment units is given at the right-hand side for comparison. Sediment units are highlighted by grey areas.

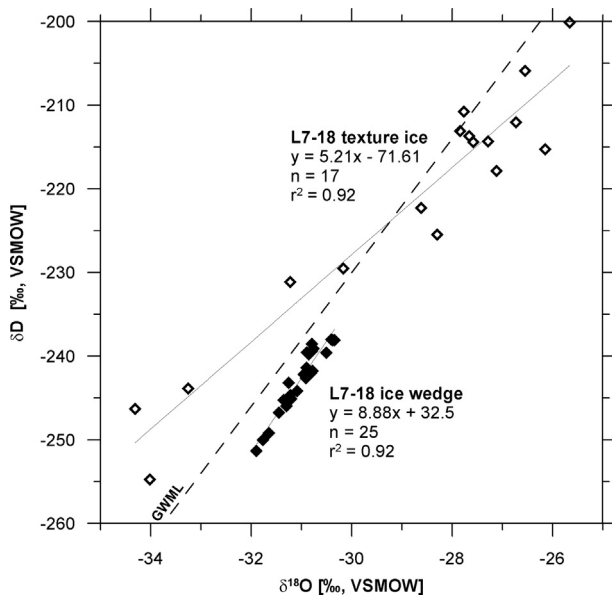


Fig. 9. $\delta^{18}\text{O}$ – δD co-isotope plot of ice wedge and texture ice of the L7-18 Molotkov (MIS3) interstadial profile with respect to the Global Meteoric Water Line (GMWL), which correlates fresh surface waters on a global scale (Craig, 1961).

5.2. Local polygon dynamics, i.e. Ice Complex formation

The studied L7-18 profile exposed at the southern coast of Bol'shoy Lyakhovsky Island reflects continuous Ice Complex accumulation and syngenetic ice-wedge growth during the Molotkov Interstadial (Table 1), a time period about 20 ka long between about 49 and 29 ka BP that contained nine meso-cycles of polygon

development. The sandy silts of the 1st cryogenic horizon (>49 ka BP) are attributed to the late Oyogos Stadial and are characterised by low ice content, high MS, low organic carbon content, and relatively heavy stable carbon isotope composition when initial polygon formation started.

The early Molotkov Interstadial (49–48 ka BP) is represented by the 2nd cryogenic horizon. Its cryolithological characteristics are rather similar to those of the 1st cryogenic horizon because this polygon developed on older deposits without distinctly altered sediment sources (Fig. 6). Afterwards, between 48 and 29 ka BP polygon development with new sedimentation took place with several alternations from subaerial to shallow subaquatic conditions. The sediment source changed as represented by decreasing MS until about 38 ka BP and became stable afterwards (Fig. 6). Variations in organic-matter properties reflect different accumulation and decomposition regimes, mainly controlled by moisture conditions in the active layer. The occurrence of peaty layers and peat lenses is mirrored by increased TOC and depleted $\delta^{13}\text{C}$ of TOC, while the highest C/N ratios point to low decomposition of organic matter likely under the anaerobic conditions of a water-saturated active layer or below a shallow polygon pond.

The highest variability in organic-matter parameters occurred between 48 and 39 ka BP during the accumulation of the 3rd–5th cryogenic horizons. Occasional wet periods very likely occurred during this time period. Such variations were probably caused by local hydrological changes of the polygonal patterned ground as described and interpreted by Minke et al. (2007) and de Klerk et al. (2011) in the Indigirka lowland from modern and Holocene polygons. Low-centred polygons with ponds could dry out or degrade into temporary high-centred polygons. A change from rather unimodal to polymodal grain-size distribution curves (Fig. 7) during the period between 39 and 29 ka BP when the 6th–8th cryogenic horizons accumulated indicates a change in the sedimentation regime. Polymodal grain-size distribution curves are

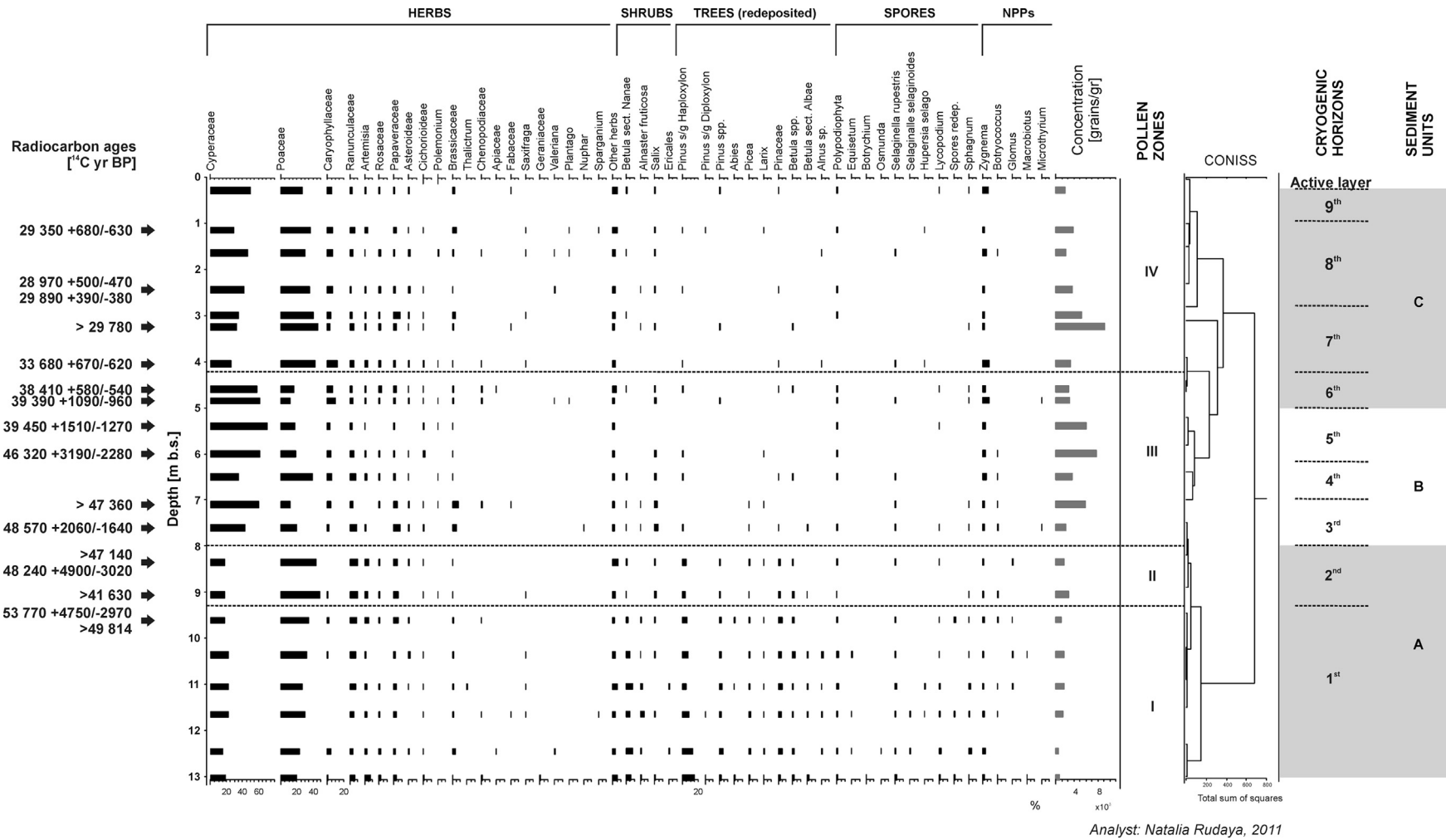


Fig. 10. Percentage diagrams of pollen and non-pollen palynomorph data from the L7-18 Molotkov (MIS3) interstadial profile. The profile zonation according to cryogenic horizons, pollen zones, and sediment units is given at the right-hand side for comparison. Sediment units are highlighted by grey areas.

rather typical of polygon deposits which accumulated on Bol'shoi Lyakhovskiy Island during the Sartan (MIS2) Stadial in a valley position between about 26 and 22 ka BP (Wetterich et al., 2011). The granulometrical data presented here most likely represent the changing sedimentation milieu as the Molotkov Interstadial waned towards the Sartan Stadial.

First of all, the polygon development between >49 and 29 ka BP as reflected by cryolithological properties and analytical data indicates stable landscape conditions of polygon tundra, sufficient winter precipitation to feed and secure the growth of syngenetic ice wedges, and internal polygon dynamics. The latter seem to depend on varying water supply in the active layer (wet vs. dry periods), changing sediment sources, peat accumulation, and variable properties of organic matter.

The cryogenic cycles are defined by their contacts with over- and underlying horizons. The position and direction of ice bands and the cryostructures between them might change from cycle to cycle, and one band might cut into another (Fig. 4). It is important to understand that the lower border of a cryogenic horizon does not necessarily correspond to a change in the sedimentation or relief conditions. Cryogenic horizons are controlled by cryogenic processes, especially by the freeze–thaw dynamics and the current position of the permafrost table. The lowermost part of a cryogenic cycle might include the uppermost part of the underlying cycle due to variations in the active-layer depth. A deepening of the active layer, as would happen below intrapolygon ponds, can thaw frozen deposits of the previous cycle, and hence alter the cryogenic structures within those deposits. Therefore, discordant contacts between distinct cryogenic horizons occur and lithological units or PZs might not correspond perfectly to cryogenic boundaries which are visible in the outcrop.

The ice-wedge stable-isotope data as temperature proxy point to stable cold winter temperatures. However, the mean $\delta^{18}\text{O}$ values of -31‰ are less depleted, by about 4‰ and 6‰ respectively, than preceding Oyogos and succeeding Sartan stadial ice wedges on Bol'shoi Lyakhovskiy Island (Andreev et al., 2009; Wetterich et al., 2011). Consequently, the mean $\delta^{18}\text{O}$ values indicating warmer winter temperatures during ice-wedge formation are consistent with the Molotkov interstadial, as indicated by the age model. The slope of 8.9 in a $\delta^{18}\text{O} - \delta\text{D}$ co-isotope plot ($n = 25$) is slightly higher than the slope of the GMWL (Fig. 9), but is clearly in the range of atmospheric precipitation as well as of other Ice Complex ice wedges on Bol'shoi Lyakhovskiy Island (Meyer and Dereviagin, 2002). The mean ice-wedge d -excess values of about 5‰ are only slightly lower than those from the Oyogos and Sartan Stadial ice wedges on Bol'shoi Lyakhovskiy Island. This implies similar late Pleistocene moisture transport patterns from either the North Atlantic Ocean or the North Pacific Ocean which are both characterised by low d -excess values as discussed in Meyer and Dereviagin (2002), Meyer (2003), and Wetterich et al. (2011).

The texture-ice isotope data exhibit an enormous scatter in both δ and d -excess values, reflecting the involvement of a variety of processes responsible for final texture ice formation. Texture ice includes varying proportions of different water sources (snow, rain, meltwater from the active layer and ice wedges) that are subject to a different number of freeze–thaw cycles and might as well also be subject to evaporation from the active layer. Moreover, fractionation during freezing has to be considered; during active-layer freezing the first ice to form has a heavier isotope composition than the last ice. The co-isotopic regression slope of 5.2 ($n = 17$, Fig. 9) is lower than the slope of 6.5 reported by Meyer and Dereviagin (2002) for texture-ice samples from different stratigraphic units at Bol'shoi Lyakhovskiy Island, and therefore points to substantial secondary fractionation effects.

The most prominent feature of the texture-ice stable isotope record is the change towards heavier $\delta^{18}\text{O}$ and δD values within the 1st and 2nd cryogenic horizon (>49–48 ka BP; Fig. 8). Considering only the marked increase in $\delta^{18}\text{O}$ (by about 9‰) and δD (by about 45‰), climate warming during the Oyogos Stadial as it waned toward the Molotkov Interstadial would be the intuitive interpretation. However, if the d -excess has also to be taken into account, this interpretation does not hold. The d -excess decreases strongly from 28‰ to 5‰ , indicating that secondary fractionation effects (i.e. during freezing) need to be considered. Furthermore, the co-isotopic regression slope (5.9) of the corresponding samples is close to a typical freezing slope and the slope of the d -excess– δD relation of -0.3 (not shown here) is typical of equilibrium freezing (see discussion in Fritz et al., 2011). Therefore, this marked isotopic change likely reflects isotope fractionation during polygon sediment freezing, mainly from above, in more or less closed-system conditions, rather than stadial-to-interstadial warming. The small variation in the texture ice $\delta^{18}\text{O}$, δD and d -excess records of unit B points to relative stable conditions, whereas the d -excess values in unit C are again highly variable and may indicate a higher proportion of summer precipitation and/or evaporation effects. However, climate variations (i.e. warming and cooling periods) should also have had an effect on the texture-ice stable-isotope records.

The studied permafrost sequence on Bol'shoi Lyakhovskiy Island dated to >49 ka and 29 ka BP reflects the paleoenvironmental history from the end of the MIS4 Stadial to the end of the MIS3 Interstadial (Fig. 11). In summary, the combined L7–18 data set allows us to identify the late Oyogos Stadial (>49 ka BP) with a quickly developing polygon tundra (1st cryogenic horizon). The PZ I pollen assemblage mirrors late stage Oyogos Stadial vegetation. Dominance of Poaceae and Cyperaceae pollen, overall low pollen concentration, numerous re-deposited conifers, and rare *Alnus* and *Betula* pollen can be characteristic regional features of that period (Andreev et al., 2011). Harsh cold and dry summers are reflected by sparse grass-sedge tundra-steppe and high amounts of redeposited conifers (PZ I). High abundance of reworked pollen reflects the erosion of older deposits confirming sparse vegetation cover (Andreev et al., 2011).

During the early Molotkov Interstadial between 49 and 48 ka BP, the polygon tundra (2nd cryogenic horizon) persists with no change in the sedimentation regime, but a distinct shift toward heaviest stable water isotope composition is seen in the texture ice records. These are interpreted to reflect changes in the freezing regime rather than in climate conditions. The pollen record of the early Molotkov Interstadial shows higher *Artemisia* counts within a grass-sedge tundra-steppe vegetation that reflected dry conditions (PZ II).

The Molotkov Interstadial optimum between 48 and 39 ka BP promoted low-centred polygon tundra with shallow water in polygon centers (3rd–6th cryogenic horizons). Higher TOC contents as well as higher C/N values from peaty deposits within the 3rd–6th cryogenic horizons point to less decomposition of organic matter and accumulation under shallow water.

PZ III correlates to the regional Molotkov Interstadial pollen assemblages. This is supported by high pollen concentration, the prevalence of sedge and grass pollen, the increase in Caryophyllaceae and *Salix* pollen abundances, and only a few reworked Pinaceae (Andreev et al., 2009). The distinctive feature of PZ III is clear dominance of Cyperaceae over Poaceae. The similar structure of pollen spectra are revealed in the several records dated as MIS3 interstadial from Bol'shoi Lyakhovskiy Island (see the details in Andreev et al., 2009) as well as in well-dated records from Bykovskiy Peninsula (Andreev et al., 2002), and Kurungnakh Island (Wetterich et al., 2008b). The indirect evidence of relatively warm climate can be a single pollen grain of *Nuphar* (water-lily). The

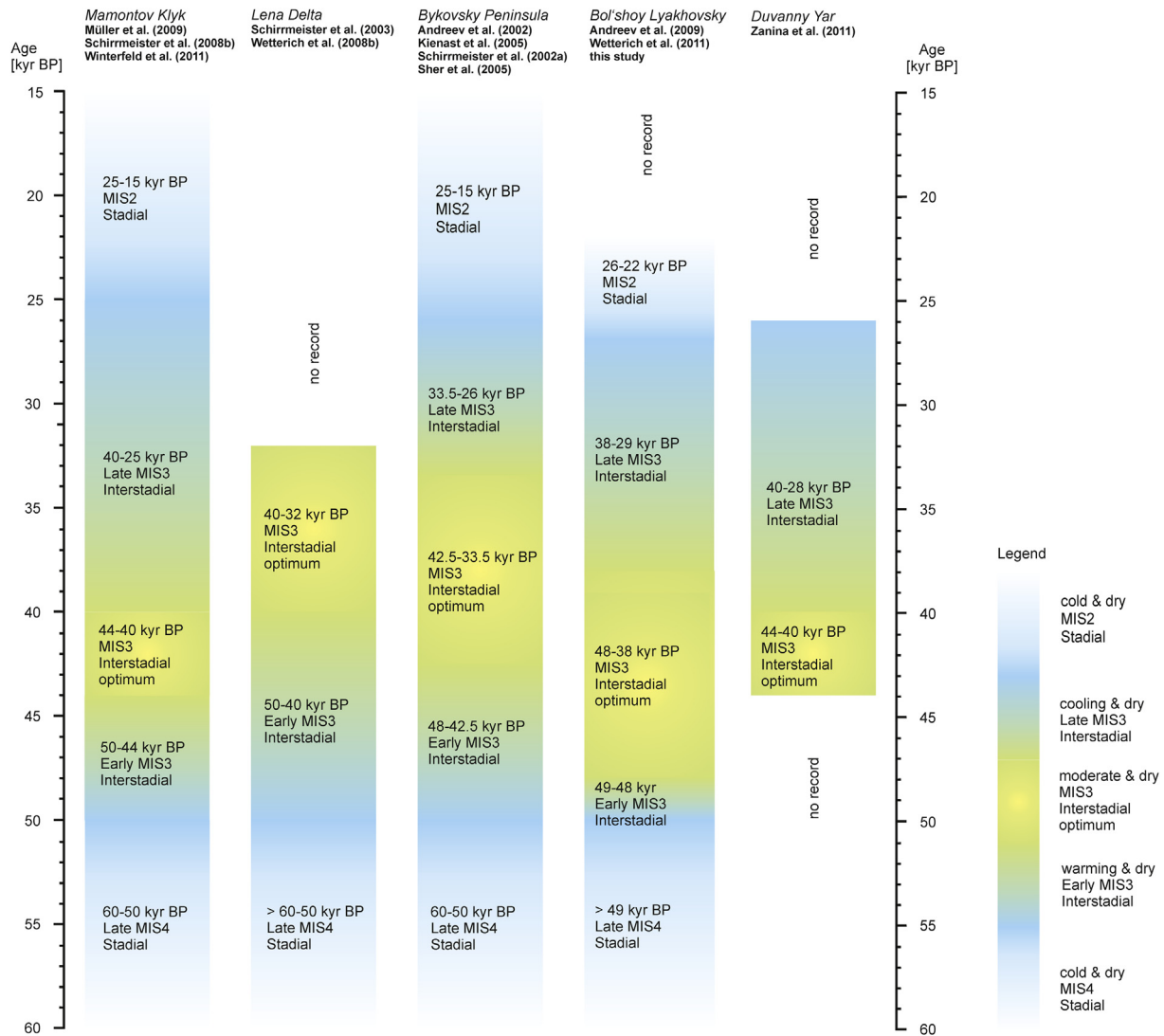


Fig. 11. Compilation scheme of summer climatic variability from MIS4 to MIS2 as inferred from five continuous Ice Complex sites in West Beringia (see also Fig. 2).

modern distribution of *Nuphar pumila* is limited to southern Yakutia and occasionally central Yakutia, the Upper Kolyma region, and the Kava River of northern Priokhot'ye. However, the numerous macrofossil remains of *Nuphar* of likely MIS3 age were found in three samples from the Abyiskaya Lowland site in the Indigirka valley (Lozhkin et al., 2011). Higher amounts of *Zygnema* (fresh-water algae) are found in PZ III and PZ IV confirming shallow-water conditions. Moister conditions in the landscape than during the previous Oyogos Stadial are assumed based on the dominance of Cyperaceae pollen while the general summer climate conditions likely remained dry, but probably slightly warmer than during the previous Stadial as reflected by higher *Salix* counts in PZ III (Andreev et al., 2011).

PZ IV can be related to the waning Molotkov Interstadial. Warmer summer air temperatures and a longer summer season would have promoted active-layer deepening, and as a consequence increased melt-water supply to the polygons on the landscape scale. The following late Molotkov period between 38 and 29 ka BP (7th–8th cryogenic horizons) still supported the occasional existence of shallow water in low-centred polygons. A cooling trend in summer air temperatures towards the end of the Interstadial can be deduced from slightly decreasing *Salix* in PZ IV

(Andreev et al., 2011), however it may be caused by changes in local vegetation structure of polygon tundra (de Klerk et al., 2011).

5.3. Regional MIS3 interstadial climate variability preserved in the Ice Complex

In a recent study, Lozhkin and Anderson (2011) suggest that the MIS3 Interstadial in Siberia presents “its own set of mysteries”, manifested in different regional palaeoclimatic trends over about 20,000 years. The paper refers to lacustrine records from East Siberia, and includes Ice Complex data from Mamontovy Khayata (Bykovsky Peninsula, Andreev et al., 2002; Sher et al., 2005) which constitute the most comprehensive permafrost record covering MIS4–MIS2. Southern and southeastern West Beringia locations in the Magadan region show a distinct MIS3 optimum with warmer and moister summers explained by higher climate instability, while northwestern West Beringia locations on Chukotka were likely warmer but consistently arid during the MIS3 (Lozhkin and Anderson, 2011). In order to expand the data base of MIS3 records preserved in the permafrost of northern West Beringia, a compilation of four more records is presented in Fig. 11. More studies have been published by Russian colleagues since the 1960s

from several locations in the East Siberian lowlands (for overview see Kaplina, 1978, 1979, 1981; Kaplina et al., 1978, 1980; Basilyan et al., 2009), but these records are rather poorly radiocarbon-dated, making it difficult to identify MIS3 periods and to compare palaeoenvironmental interpretation from the data.

The spatial coverage of the data presented here ranges from the Lena-Anabar lowland (Cape Mamontov Klyk) in the west to the Kolyma lowland (Duvanny Yar) in the east (Fig. 2). In addition to data from Bol'shoy Lyakhovsky Island, permafrost records covering the MIS3 Interstadial (Fig. 11) were studied at the Duvanny Yar exposure (Zanina et al., 2011 and references therein), on Bykovsky Peninsula (Schirrmeister et al., 2002a; Kienast et al., 2005; Sher et al., 2005), on Kurungnakh Island in the central Lena Delta (Schirrmeister et al., 2003; Wetterich et al., 2008b), and at Cape Mamontov Klyk (Schirrmeister et al., 2008b; Müller et al., 2009; Winterfeld et al., 2011). In these records, the MIS3 onset with a transition from the previous MIS4 Stadial (not recorded at Duvanny Yar) starts between >49 ka BP (on Bol'shoy Lyakhovsky Island) and 48 ka BP (on Bykovsky Peninsula). The MIS3 termination (not recorded on Kurungnakh Island) took place between 28 ka BP (at Duvanny Yar) and 26 ka BP (on Bykovsky Peninsula). The identification of MIS3 optima is based mainly on pollen data (Andreev et al., 2011 and references therein), but if available also on other proxy datasets (e.g. plant macrofossils from Bykovsky Peninsula, Kienast et al., 2005; testate amoebae from Bykovsky Peninsula, Bobrov et al., 2004; Cape Mamontov Klyk, Müller et al., 2009; ostracods from Bykovsky Peninsula, Wetterich et al., 2005; and Kurungnakh Island, Wetterich et al., 2008b). Ice-wedge stable isotope data from Bykovsky Peninsula have been interpreted as proxy for winter conditions; pointing to less severe air temperatures around 42 ka BP (Meyer et al., 2002). Warmer summer air temperatures and moister conditions on the landscape scale during the MIS3 optimum are deduced mainly from *Salix* and green algae findings in the palynological tundra-steppe records (Andreev et al., 2011); high diversity and abundance of testate amoebae and ostracods (Bobrov et al., 2004; Wetterich et al., 2005), and high percentages of xerophilous steppe insects (Sher et al., 2005) confirm this interpretation. The MIS3 optimum period is characterised by a peak of the Mammoth Fauna (Sher et al., 2005). The onset, duration, and termination of the MIS3 Interstadial optimum vary in the different records (Fig. 11). Rather short periods between 44 and 40 ka BP are interpreted from the Duvanny Yar and Cape Mamontov Klyk records while Bykovsky Peninsula and Bol'shoy Lyakhovsky Island data show longer periods between 42.5 and 33.5 ka BP and 48 and 38 ka BP, respectively. The Ice Complex palaeoenvironmental archive exhibits late Quaternary stadial-interstadial climate variability for West Beringia in millennial resolution. Differences in local records might indeed be caused by different past climate conditions on a local scale and/or induced by sample resolution and geochronological control. In this context, the Bol'shoy Lyakhovsky record provides additional strong evidence for interstadial climate variability in the northern part of West Beringia as was first suggested by Kind (1974) (see also Anderson and Lozhkin, 2001; Lozhkin and Anderson, 2011). In this work at least five periods are differentiated for the MIS3 Interstadial of which the optimum period is also seen in the interstadial Ice Complex of Bol'shoy Lyakhovsky Island (Fig. 11). Early and late MIS3 warm intervals are not recorded.

6. Conclusions

During the MIS3 Molotkov Interstadial, continuous Ice Complex formation took place on Bol'shoy Lyakhovsky Island. The development of polygon tundra formed nine cryogenic horizons and reflects the local landscape evolution, i.e. polygon dynamics during the Last Glacial period. A generally stable landscape of a wide,

gently sloping, and segmented accumulation plain is assumed as the formation area of the MIS3 Ice Complex on Bol'shoy Lyakhovsky Island. Changes in the accumulation conditions are indicated at the end of the MIS3 in transition to the MIS2. The latter is locally preserved in valley deposits cutting the MIS3 Ice Complex as described by Wetterich et al. (2011). Polygon dynamics during MIS3 affected the palaeoenvironmental archive of Ice Complex deposits with interference between and overlapping of several proxy records. By the use of combined cryolithological, sedimentological, geochemical, geochronological, and palaeontological proxy data, MIS3 Interstadial climate variability was elucidated. The MIS3 climate optimum between about 48 and 38 ka BP as inferred from Ice Complex on Bol'shoy Lyakhovsky Island adds another record of MIS3 climate variability in West Beringia.

Acknowledgements

The study presented here is part of the Russian–German *System Laptev Sea* cooperative scientific effort, and the International Polar Year *Past Permafrost* project (IPY project 15). The study was conducted under the auspices of the joint Russian–German *Polygons in tundra wetlands: State and dynamics under climate variability in polar regions* project (Russian Foundation for Basic Research, RFBR grant No 11-04-91332-NNIO-a and Deutsche Forschungsgemeinschaft, DFG grant \mathcal{N}° HE 3622-16-1). This study is furthermore a contribution to the *Eurasian Arctic Ice 4k* project (DFG grant No OP 217/2-1). We thank our colleagues who helped during fieldwork in 2007, especially Dmitry Dobrynin from Moscow State University. We are grateful to Dmitry Mel'nichenko and colleagues from the Hydrobase Tiksi, and Waldemar Schneider from AWI Potsdam who greatly supported the logistics of this expedition, and also to the team of Fedor Selyakhov from the Lena Delta Reserve who hosted our field camp at the Zimov'e River mouth in July 2007. The analytical work in the AWI laboratories was expertly conducted by Ute Bastian and Lutz Schönicke. The identification of plant remains for radiocarbon dating was conducted by Frank Kienast (Senckenberg Weimar) and Romy Zibulski (AWI Potsdam). Finally, the paper benefited by constructive comments and English language correction from Candace O'Connor (University of Alaska Fairbanks) as well as from two reviewers.

Appendix A. Supplementary data

Supplementary data related to this article can be found at <http://dx.doi.org/10.1016/j.quascirev.2013.11.009>.

References

- Anderson, P.M., Lozhkin, A.V., 2001. The Stage 3 interstadial complex (Karginiskii/middle Wisconsinan interval) of Beringia: variations in paleoenvironments and implications for paleoclimatic interpretations. *Quat. Sci. Rev.* 20, 93–125. [http://dx.doi.org/10.1016/S0277-3791\(00\)00129-3](http://dx.doi.org/10.1016/S0277-3791(00)00129-3).
- Andreev, A.A., Schirrmeister, L., Siegert, C., Bobrov, A.A., Demske, D., Seiffert, M., Hubberten, H.-W., 2002. Paleoenvironmental changes in Northeastern Siberia during the Late Quaternary – evidence from pollen records of the Bykovsky Peninsula. *Polarforschung* 70, 13–25.
- Andreev, A.A., Grosse, G., Schirrmeister, L., Kuzmina, S.A., Novenko, E.Yu., Bobrov, A.A., Tarasov, P.E., Kuznetsova, T.V., Krbetschek, M., Meyer, H., Kunitsky, V.V., 2004. Late Saalian and Eemian palaeoenvironmental history of the Bol'shoy Lyakhovsky Island (Laptev Sea region, Arctic Siberia). *Boreas* 33, 319–348. <http://dx.doi.org/10.1080/03009480410001974>.
- Andreev, A.A., Grosse, G., Schirrmeister, L., Kuznetsova, T.V., Kuzmina, S.A., Bobrov, A.A., Tarasov, P.E., Novenko, E.Yu., Meyer, H., Derevyagin, A.Yu., Kienast, F., Bryantseva, A., Kunitsky, V.V., 2009. Weichselian and Holocene palaeoenvironmental history of the Bol'shoy Lyakhovsky Island, New Siberian Archipelago, Arctic Siberia. *Boreas* 38, 72–110. <http://dx.doi.org/10.1111/j.1502-3885.2008.00039.x>.
- Andreev, A., Schirrmeister, L., Tarasov, P.E., Ganopolski, A., Brovkin, V., Siegert, C., Wetterich, S., Hubberten, H.-W., 2011. Vegetation and climate history in the Laptev Sea region (Arctic Siberia) during Late Quaternary inferred from pollen

- records. *Quat. Sci. Rev.* 30, 2182–2199. <http://dx.doi.org/10.1016/j.quascirev.2010.12.026>.
- Basilyan, A.E., Anisimov, M.A., Pavlova, E.Yu., Pitulko, V.V., Nikolskiy, P.A., 2009. Oporniy razrez kvartera Yano-Indigirskoi nizmenosti v nizhnem techenii reki Yana (Base reference section of Quaternary deposits for the Yana-Indigirka lowland in the Yana River downstream area). In: Kontorovich, A.E., Volkova, V.S., Khazina, I.V., Khazin, L.B. (Eds.), *Proceedings of the 6th All-Russian Quaternary Conference*. RAS SB Publishers, Novosibirsk, pp. 63–65 (in Russian).
- Beug, H.-J., 2004. *Leitfaden der Pollenbestimmung für Mitteleuropa und angrenzende Gebiete*. Verlag Dr. Friedrich Pfeil, Munich.
- Blinnikov, M.S., Gaglioti, B.V., Walker, D.A., Wooller, M.J., Zazula, G.D., 2011. Pleistocene graminoid-dominated ecosystems in the Arctic. *Quat. Sci. Rev.* 30, 2906–2929. <http://dx.doi.org/10.1016/j.quascirev.2011.07.002>.
- Blott, S.J., Pye, K., 2001. GRADISTAT: a grain size distribution and statistics package for the analysis of unconsolidated sediments. *Earth Surf. Process. Landf.* 26, 1237–1248. <http://dx.doi.org/10.1002/esp.261>.
- Bobrov, A.A., Andreev, A.A., Schirmermeister, L., Siegert, C., 2004. Testate amoebae (Protozoa: Testacealobosea and Testaceafilosea) as bioindicators in the Late Quaternary deposits of the Bykovsky Peninsula, Laptev Sea, Russia. *Palaeogeogr. Palaeoclimatol. Palaeoecol.* 209, 165–181. <http://dx.doi.org/10.1016/j.palaeo.2004.02.012>.
- Bunge, A.A., 1887. Bericht ueber den fernerer Gang der Expedition. Reise nach den Neusibirischen Inseln. Aufenthalt auf der Grossen Ljachof-Insel. In: Schrenk, L.V., Maximovicz, C.J. (Eds.), *Expedition zu den Neusibirischen Inseln und dem Jana-Lande (1885)*. Beitrage zur Kenntnis des russischen Reiches und der angrenzenden Laender, vol. III, pp. 231–284 (in German).
- Craig, H., 1961. Isotopic variations in meteoric waters. *Science* 133, 1702–1703. <http://dx.doi.org/10.1126/science.133.3465.1702>.
- de Klerk, P., Donner, N., Karpov, N.S., Minke, M., Joosten, H., 2011. Short-term dynamics of a low-centred ice-vedge polygon near Chokurdakh (NE Yakutia, NE Siberia) and climate change during the last ca 1250 years. *Quat. Sci. Rev.* 30, 3013–3031. <http://dx.doi.org/10.1016/j.quascirev.2011.06.016>.
- Fægri, K., Iversen, J., 1989. *Textbook of Pollen Analysis*, fourth ed. John Wiley & Sons, Chichester.
- Fritz, M., Wetterich, S., Meyer, H., Schirmermeister, L., Lantuit, H., Pollard, W.H., 2011. Origin and characteristics of massive ground ice on Herschel Island (western Canadian Arctic) as revealed by stable water isotope and hydrochemical signatures. *Permafrost Periglac. Process.* 22, 26–38. <http://dx.doi.org/10.1002/ppp.714>.
- Fritz, M., Wetterich, S., Schirmermeister, L., Meyer, H., Lantuit, H., Preusser, F., Pollard, W.H., 2012. Eastern Beringia and beyond: Late Wisconsinan and Holocene landscape dynamics along the Yukon Coastal Plain, Canada. *Palaeogeogr. Palaeoclimatol. Palaeoecol.* 319–320, 28–45. <http://dx.doi.org/10.1016/j.palaeo.2011.12.015>.
- Geyh, M.A., 2001. Reflections on the $^{230}\text{Th}/\text{U}$ dating of dirty material. *Geochronometria* 20, 9–14.
- Giterman, R.E., 1985. *Istoriya rastitel'nosti severo-vostoka SSSR v Pliotsene i Pleistotsene (The vegetation history of the north-eastern USSR during the Pliocene and Pleistocene)*. Nauka, Moscow, p. 92 (in Russian).
- Grichuk, M.P., Grichuk, V.O., 1960. O prilednikovoi rastitel'nosti na territoriyakh SSSR (Periglacial vegetation of the USSR). In: *Trudy Instituta Geografii AN SSSR (Proceedings of the Institute of Geography, USSR Academy of Sciences)*, vol. 80, pp. 66–100.
- Grimm, E.C., 1991. *TILIAGRAPH v1.25*. Illinois State Museum, Research and Collections Center, Springfield IL.
- Grimm, E.C., 2004. *TGView 2.0.2 (Software)*. Illinois State Museum, Research and Collections Center, Springfield, IL.
- Grosse, G., Robinson, J.E., Bryant, R., Taylor, M.D., Harper, W., DeMasi, A., Kyker-Snowman, E., Veremeeva, A., Schirmermeister, L., Harden, J., 2013. Distribution of Late Pleistocene Ice-rich Syngenetic Permafrost of the Yedoma Suite in East and Central Siberia, Russia. *U.S. Geological Survey Open File Report 2013-1078*, p. 37.
- Groote, P.M., Nadeau, M.J., Rieck, A., 2004. ^{14}C -AMS at the Leibniz-Labor: radiometric dating and isotope research. *Nucl. Instr. Methods Phys. Res. Sect. B* 223–224, 55–61. <http://dx.doi.org/10.1016/j.nimb.2004.04.015>.
- Groote, P., Nadeau, M.-J., Hüls, C.M., Rakowski, A., 2011. Organic backgrounds: are they material dependent? In: *Programme and Abstracts Handbook of the 12th International Conference on Accelerator Mass Spectrometry (AMS-12)*, 20–25 March 2011, Wellington, New Zealand, p. 244.
- Grosse, G., Romanovsky, V.E., Jorgenson, T., Walter Anthony, K., Brown, J., Overduin, P.P., 2011a. Vulnerability and feedbacks of permafrost to climate change. *Eos Trans. AGU* 92 (9), 73–74.
- Grosse, G., Harden, J., Turetsky, M., McGuire, A.D., Camill, P., Tarnocai, C., Frolking, S., Schuur, E.A.G., Jorgenson, T., Marchenko, S., Romanovsky, V., Wickland, K.P., French, N., Waldrop, M., Bourgeau-Chavez, L., Striegl, R.G., 2011b. Vulnerability of high latitude soil carbon in North America to disturbance. *J. Geophys. Res.* – Biogeosci. 116, G00K06. <http://dx.doi.org/10.1029/2010JG001507>.
- Gubin, S.V., 1994. Pozdnepleistotsenovo pochvoobrazovanie na primorskikh nizmenostyakh severa Yakutii (Late Pleistocene pedogenesis in coastal lowlands of Northern Yakutia). *Pochvovedenie (Soil Sci.)* 8, 5–14 (in Russian).
- Gubin, S.V., Veremeeva, A.A., 2010. Parent materials enriched in organic matter in the Northeast of Russia. *Eurasian Soil Sci.* 43, 1238–1243. <http://dx.doi.org/10.1134/S1064229310110062>.
- Hobbies, J.E. (Ed.), 1980. *Limnology of Tundra Ponds, Barrow, Alaska*. US/IBP Synthesis Series, vol. 13. Dowden, Hutchinson and Ross, Stroufburg PA.
- Ilyashuk, B.P., Andreev, A.A., Bobrov, A.A., Tumskey, V.E., Ilyashuk, E.A., 2006. Interglacial history of a palaeo-lake and regional environment: a multi-proxy study of a permafrost deposit from Bol'shoy Lyakhovskiy Island, Arctic Siberia. *J. Paleolimnol.* 35, 855–872. <http://dx.doi.org/10.1007/s10933-005-5859-6>.
- Ivanov, O.A., 1972. Stratigrafiya i korrelyatsiya neogenovykh i chetvertichnykh otlozhenii subarkticheskikh ravnin Vostochnoi Yakutii (Stratigraphy and correlation of Neogene and Quaternary deposits of subarctic plains in Eastern Yakutia). In: *Problemy izucheniya chetvertichnogo perioda (Problems of the Study of Quaternary Period)*. Nauka, Moscow, pp. 202–211 (in Russian).
- Jankovska, V., 1991. Unbekannte Objekte in Pollenpräparaten. Tardigrada. In: *Proceedings of the Pan-European Palaeobotany Conference*, Vienna, pp. 19–23.
- Jørgensen, T., Haile, J., Möller, P., Andreev, A., Boessenkool, S., Rasmussen, M., Kienast, F., Coissac, E., Taberlet, P., Brochmann, C., Bigelow, N.H., Andersen, K., Orlando, L., Gilbert, M.T.P., Willerslev, E., 2012. A comparative study of ancient sedimentary DNA, pollen and macrofossils from permafrost sediments of northern Siberia reveals long-term vegetational stability. *Mol. Ecol.* 21, 1989–2003. <http://dx.doi.org/10.1111/j.1365-294X.2011.05287.x>.
- Kaplina, T.N., 1978. Skorosti nakopleniya i vozrast Ledovogo Kompleksa primorskikh nizmenostei Yakutii (Accumulation rates and age of the Ice Complex in the northern lowlands of Yakutia). *Merzl. Issled. (Permafrost Res.)* XVII, 142–147 (in Russian).
- Kaplina, T.N., 1979. Sporovo-pyl'tsevye spektry osadkov Ledovogo Kompleksa primorskikh nizmenostei Yakutii (Palynological spectra of Ice Complex deposits in the northern lowlands of Yakutia). *Izv. Akad. Nauk SSSR – Seriya Geogr. (Notes USSR Acad. Sci. – Geogr.)* 2, 85–93 (in Russian).
- Kaplina, T.N., 1981. Istoriya merzlykh tolscheg severnoi Yakutii v pozdnom Kainozoe (History of late Cenozoic frozen horizons in northern Yakutia). In: *Istoriya pazvitiya mnogoletnemerzlykh porod Evrazii (History of Eurasian Permafrost Development)*. Nauka, Moscow, pp. 153–181 (in Russian).
- Kaplina, T.N., Giterman, R.E., Lakhtina, O.V., Abrashov, B.A., Kiselev, S.V., Sher, A.V., 1978. Duvanny Yar – oporniy razrez pozdnepleistotsenovykh otlozhenii Kolymskoi nizmenosti (Duvanny Yar – a key section of Upper Pleistocene deposits of the Kolyma lowland). *Byulleten' Kom. po Izucheniyu Chetvertichnogo Perioda (Bull. Quat. Res. Comm.)* 48, 49–65 (in Russian).
- Kaplina, T.N., Sher, A.V., Giterman, R.E., Zazhigin, V.S., Kiselev, C.V., Lozhkin, A.V., Nikitin, V.P., 1980. Oporniy razrez pleistotsenovykh otlozhenii na r. Allaikha, nizov'ya Indigirki (Key site of Pleistocene deposits at the Allaikha River, Indigirka lowland). *Byulleten' Kom. po Izucheniyu Chetvertichnogo Perioda (Bull. Quat. Res. Comm.)* 50, 73–95 (in Russian).
- Kerfoot, D.E., 1972. Thermal contraction cracks in an arctic tundra environment. *Arctic* 25, 142–150.
- Kienast, F., Schirmermeister, L., Siegert, C., Tarasov, P., 2005. Palaeobotanical evidence for warm summers in the East Siberian Arctic during the last cold stage. *Quat. Res.* 63, 283–300. <http://dx.doi.org/10.1016/j.yqres.2005.01.003>.
- Kind, N.V., 1974. Geokhologiya pozdnogo antropogena po izotopnym dannym (Late Quaternary geochronology according to isotope data). *Nauka, Moscow*, p. 256 (in Russian).
- Kiselev, S.V., Nazarov, V.I., 2009. Late Cenozoic insects of northern Eurasia. *Paleontol. J.* 43 (7), 723–850. <http://dx.doi.org/10.1134/S0031030109070016>.
- Konishchev, V.N., Kolesnikov, S.F., 1981. Osobennosti stroeniya i sostava pozdne-kainozoiskikh otlozheniyakh v obnazhenii Oyogosskii Yar (Peculiarities of structure and composition of late Cenozoic deposits in the section of Oyogosskii Yar). *Probl. kriolitologii (Probl. of Cryolithol.)* IX, 107–117 (in Russian).
- Kunitsky, V.V., 1998. Ledoviy kompleks i krioplanatsionnye terrassy na ostrove Bol'shoy Lyakhovskiy (Ice Complex and cryoplanation terraces on Bol'shoy Lyakhovskiy Island). In: Kamensky, R.M., Kunitsky, V.V., Olovin, B.A., Shepelev, V.V. (Eds.), *Problemy Geokriologii (Problems of Geocryology)*. RAS SB Permafrost Institute, Yakutsk, pp. 60–72 (in Russian).
- Kupriyana, L.A., Alyoshina, L.A., 1972. Pyl'za i spory rastenii flory Evropeiskoi chasti SSSR (Pollen and spores of plant from the European part of the USSR). *Nauka, Leningrad* (in Russian).
- Lachenbruch, A.H., 1962. Mechanics of thermal contraction cracks and ice-wedge polygons in permafrost. *Geol. Soc. America Spec. Paper* 70, 1–69.
- Leffingwell, E., de K., 1915. Ground ice-wedges. The dominant form of ground ice on the north coast of Alaska. *J. Geol.* 23, 635–654. <http://dx.doi.org/10.1086/622281>.
- Lozhkin, A.V., Anderson, P.M., 2011. Forest or no forest: implications of the vegetation record for climatic stability in Western Beringia during Oxygen Isotope Stage 3. *Quat. Sci. Rev.* 30, 2160–2181. <http://dx.doi.org/10.1016/j.quascirev.2010.12.022>.
- Lozhkin, A.V., Anderson, P.M., Vazhenina, L.N., 2011. Younger Dryas and Early Holocene Peats from northern Far East Russia. *Quat. Int.* 237, 54–64. <http://dx.doi.org/10.1016/j.quaint.2011.01.009>.
- Meyer, H., 2003. Late Quaternary climate history of Northern Siberia – evidence from ground ice. *Berichte zur Polar- und Meeresforsch.* 461, 1–109.
- Meyer, H., Schönicke, L., Wand, U., Hubberten, H.-W., Friedrichsen, H., 2000. Isotope studies of hydrogen and oxygen in ground ice – experiences with the equilibration technique. *Isot. Environ. Health Stud.* 36, 133–149. <http://dx.doi.org/10.1080/10256010008032939>.
- Meyer, H., Dereviagin, A.Yu., Siegert, C., Hubberten, H.-W., 2002. Paleoclimate studies on Bykovsky Peninsula, North Siberia – hydrogen and oxygen isotopes in ground ice. *Polarforschung* 70, 37–51.
- Meyer, H., Dereviagin, A.Yu., Siegert, C., Schirmermeister, L., Hubberten, H.-W., 2002. Paleoclimate reconstruction on Big Lyakhovskiy Island, North Siberia – hydrogen and oxygen isotopes in ice wedges. *Permafrost Periglac. Process.* 13, 91–105. <http://dx.doi.org/10.1002/ppp.416>.

- Minke, M., Donner, N., Karpov, N.S., de Klerk, P., Joosten, H., 2007. Distribution, diversity, development and dynamics of polygon mires: examples from Northeast Yakutia (Siberia). *Peatl. Int.* 2007 (1), 36–40.
- Müller, S., Bobrov, A.A., Schirmermeister, L., Andreev, A.A., Tarasov, P.E., 2009. Testate amoebae record from the Laptev Sea coast and its implication for the reconstruction of Late Pleistocene and Holocene environments in the Arctic Siberia. *Palaeogeogr. Palaeoclimatol. Palaeoecol.* 271, 301–315. <http://dx.doi.org/10.1016/j.palaeo.2008.11.003>.
- Nadeau, M.-J., Schleicher, M., Grootes, P.M., Erlenkeuser, H., Gott dang, A., Mous, D.J.W., Sarnthein, M., et al., 1997. The Leibniz-Labor AMS facility at the Christian-Albrechts University, Kiel, Germany. *Nucl. Instr. Methods Phys. Res. Sect. B123*, 22–30.
- Nadeau, M., Grootes, P.M., Schleicher, M., Hasselberg, P., Rieck, A., Bitterling, M., 1998. Sample throughput and data quality at the Leibniz-Labor AMS facility. *Radiocarbon* 40, 239–245.
- Nadeau, M.-J., Grootes, P.M., Voelker, A., Bruhn, F., Duhr, A., Oriwall, A., 2001. Carbonate ^{14}C Background: does it have multiple personalities. *Radiocarbon* 43, 169–176.
- Nikolskiy, P.A., Basilyan, A.E., 2004. Mys Svyatoi Nos - oporniy razrez chetvertichnykh otlozhenii severa Yano-Indigirskoi nizmenosti (Cape Syatoi Nos - a key section of Quaternary deposits of the Yana-Indigirka lowland). In: Nikolskiy, P.A., Pitulko, V.V. (Eds.), *Estestvennaya istoriya rossiiskoi vostochnoi Arktiki v pleitotsene i golotsene (The Pleistocene and Holocene natural history of the Russian Eastern Arctic)*. GEOS, Moscow, pp. 5–13 (in Russian).
- Nikolskiy, P.A., Sulerzhitskiy, L.D., Pitulko, V.V., 2011. Last straw versus Blitzkrieg overkill: climate-driven changes in the Arctic Siberian mammoth population and the Late Pleistocene extinction problem. *Quat. Sci. Rev.* 30, 2309–2328. <http://dx.doi.org/10.1016/j.quascirev.2010.10.017>.
- Opel, T., Dereviagin, A., Meyer, H., Schirmermeister, L., Wetterich, S., 2011. Paleoclimatic information from stable water isotopes of Holocene ice wedges at the Dmitrii Laptev Strait (Northeast Siberia). *Permafrost Periglac. Process.* 22, 84–100. <http://dx.doi.org/10.1002/ppp.667>.
- Popov, A.I., 1978. Cryolithogenesis, the composition and structure of frozen rocks and ground ice. *Biuletyn Perylglac.* 21, 155–170.
- Prokhorova, C.M., Ivanov, O.A., 1973. Olovonosnye granitoidy Yano-Indigirskoi nizmenosti i svyazannye s nimi possypi (Tin-bearing granitoids of the Yana-Indigirka lowland and related deposits). In: *Trudy nauchno-issledovatel'skogo Instituta Geologii Arktiki (Transactions of the Research Institute of Arctic Geology)*. Nedra, Leningrad, pp. 152–205 (in Russian).
- Romanovskii, N.N., 1958. Hovye dannye o stroenii chetvertichnykh otlozhenii ostrova Bol'shoy Lyakhovskiy, Novosibirskie Ostovava (New data about the structure of Quaternary deposits of Bol'shoy Lyakhovskiy Island, New Siberian Islands). *Nauchnye Doklady Vyss. Shkoly. Seriya Geol.-Geogr. (Sci. Trans. Higher Educ. - Geol.-Geogr.)* 2, 243–248 (in Russian).
- Romanovskii, N.N., 1977. Formirovaniye polygonal'no-zhil'nykh struktur (Formation of polygonal-wedge systems). *Nauka, Novosibirsk*, p. 215 (in Russian).
- Romanovskii, N.N., 1993. *Osnovy kriolitogeneza litosfery (Basic concepts of cryogenesis in the lithosphere)*. Moscow University Press, p. 336 (in Russian).
- Romanovskii, N.N., Hubberten, H.-W., Gavrilov, A.V., Tumskey, V.E., Kholodov, A.L., 2004. Permafrost of the east Siberian Arctic shelf and coastal lowlands. *Quat. Sci. Rev.* 23, 1359–1369. <http://dx.doi.org/10.1016/j.quascirev.2003.12.014>.
- Schirmermeister, L., Siegert, C., Kuznetsova, T., Kuzmina, S., Andreev, A.A., Kienast, F., Meyer, H., Bobrov, A.A., 2002a. Paleoenvironmental and paleoclimatic records from permafrost deposits in the Arctic region of Northern Siberia. *Quat. Int.* 89, 97–118. <http://dx.doi.org/10.1016/j.quaint.2010.04.004>.
- Schirmermeister, L., Oezen, D., Geyh, M.A., 2002b. $^{230}\text{Th}/\text{U}$ dating of frozen peat, Bol'shoy Lyakhovskiy Island (North Siberia). *Quat. Res.* 57, 253–258. <http://dx.doi.org/10.1006/qres.2001.2306>.
- Schirmermeister, L., Kunitsky, V.V., Grosse, G., Schwamborn, G., Andreev, A.A., Meyer, H., Kuznetsova, T., Bobrov, A., Oezen, D., 2003. Late Quaternary history of the accumulation plain north of the Chekanovsky Ridge (Lena Delta, Russia) – a multidisciplinary approach. *Polar Geogr.* 27, 277–319. <http://dx.doi.org/10.1080/0789610225>.
- Schirmermeister, L., Wetterich, S., Tumskey, V., Dobrynin, D., 2008a. *Palaeoenvironmental studies on Bol'shoy Lyakhovskiy Island*. *Berichte zur Polar und Meeresforsch.* 584, 51–84.
- Schirmermeister, L., Grosse, G., Kunitsky, V., Magens, D., Meyer, H., Dereviagin, A., Kuznetsova, T., Andreev, A., Babiy, O., Kienast, F., Grigoriev, M., Overduin, P.P., Preusser, F., 2008b. Periglacial landscape evolution and environmental changes of Arctic lowland areas for the last 60,000 years (Western Laptev Sea coast, Cape Mamontov Klyk). *Polar Res.* 27, 249–272. <http://dx.doi.org/10.1111/j.1751-8369.2008.00067.x>.
- Schirmermeister, L., Kunitsky, V., Grosse, G., Wetterich, S., Meyer, H., Schwamborn, G., Babiy, O., Dereviagin, A., Siegert, C., 2011a. Sedimentary characteristics and origin of the Late Pleistocene Ice Complex on north-east Siberian Arctic coastal lowlands and islands – a review. *Quat. Int.* 241, 3–25. <http://dx.doi.org/10.1016/j.quaint.2010.04.004>.
- Schirmermeister, L., Grosse, G., Wetterich, S., Overduin, P., Strauss, J., Schuur, E.A.G., Hubberten, H.-W., 2011b. Fossil organic matter characteristics in permafrost deposits of the Northeast Siberian Arctic. *J. Geophys. Res. - Biogeosci.* 116, G00M02. <http://dx.doi.org/10.1029/2011JG001647>.
- Schirmermeister, L., Froese, D., Tumskey, V., Grosse, G., Wetterich, S., 2013. Yedoma: Late Pleistocene ice-rich syngenetic permafrost of Beringia (Chapter 6.12). In: Elias, S.A. (Ed.), *The Encyclopedia of Quaternary Science*, second ed., vol. 3. Elsevier, Amsterdam, pp. 542–552.
- Sher, A.V., 1971. Mlekopitayushchie i stratigrafiya pleitotsena krainego severo-vostoka SSSR i severnoi Ameriki (Mammals and stratigraphy of the Pleistocene of the far Northeast of the USSR and northern America). *Nauka, Moscow*, p. 310 (in Russian).
- Sher, A.V., 1997. Yedoma as a store of paleoenvironmental records in Beringia. In: Elias, S., Brigham-Grette, J. (Eds.), *Abstracts and Program of the Beringia Paleoenvironmental Workshop*. September 20–23, 1997, Florissant, Colorado, pp. 92–94.
- Sher, A.V., Kuzmina, S.A., Kuznetsova, T.V., Sulerzhitskiy, L.D., 2005. New insights into the Weichselian environment and climate of the East Siberian Arctic, derived from fossil insects, plants, and mammals. *Quat. Sci. Rev.* 24, 533–569. <http://dx.doi.org/10.1016/j.quascirev.2004.09.007>.
- Shilo, N.A. (Ed.), 1987. Resheniya mezhdovomsvennogo stratigraficheskogo soveshchaniya po chetvertichnoi sisteme vostoka SSSR. Ob'yasnitel'nye zapiski k regional'nym skhemam chetvertichnykh otlozhenii vostoka SSSR (Decisions of the Inter-institutional Stratigraphic Summit of the Quaternary System of the Eastern Part of the USSR, 1987. Explanatory Notes for Regional Stratigraphic Schemes of Quaternary Deposits of the Eastern Part of the USSR). Severo-vostochnyi kompleksnyi nauchnoissledovatel'skii Institut, Dal'nevostochnoe Otdelenie Akademii nauk SSSR, Magadan (USSR Academy of Sciences FEB NEISRI, Magadan), pp. 29–69 (in Russian).
- Shkatova, V.G., 2011. Sostoyanie stratigraficheskoi bazy kvartera territorii Rossii i osnovnye zadachi po ee uovershenstvovaniyu (The state of the Russian Quaternary stratigraphic base and main tasks for its improvement). In: Korsakova, O.P., Kol'ka, V.V. (Eds.), *Proceedings of the 7th All-Russian Quaternary Conference*, vol. 2. RAS Geological Institute of the Kola Science Center, Apatity, pp. 326–328 (in Russian).
- Slagoda, E.A., 2004. Kriolitogennyye otlozheniya Primorskoi ravniny morya Laptevykh: litologiya i mikromorfologiya (Cryolithogenic deposits of the Laptev Sea coastal plain: lithology and micromorphology). *Ekspres, Tyumen*, p. 119 (in Russian).
- Stockmarr, J., 1971. Tablets with spores used in absolute pollen analysis. *Pollen et Spores* 13, 615–621.
- Strauss, J., Schirmermeister, L., Wetterich, S., Borchers, A., Davydov, S.P., 2012. Grain-size properties and organic-carbon stock of Yedoma Ice Complex permafrost from the Kolyma lowland, Northeastern Siberia. *Glob. Biochem. Cycles* 26, GB3003. <http://dx.doi.org/10.1029/2011GB004104>.
- Strauss, J., Schirmermeister, L., Grosse, G., Wetterich, S., Ulrich, M., Hubberten, H.-W., 2013. The deep permafrost carbon pool of the Yedoma region in Siberian and Alaska. *Geophys. Res. Lett.* (submitted for publication).
- Stuiver, M., Polach, H.A., 1977. Discussion: reporting of ^{14}C data. *Radiocarbon* 19 (3), 355–363.
- Tumskey, V.E., 2012. Osobennosti kriolitogeneza otlozhenii severnoi Yakutii v srednem Neopleistotsene – Golotsene (Peculiarities of cryolithogenesis in northern Yakutia from the Middle Neopleistocene to the Holocene). *Kriosfera Zemli (Earth's Cryosphere)* 16, 12–21 (in Russian).
- Tumskey, V.E., Basilyan, A.E., 2006. Key section of Quaternary deposits on Bol'shoy Lyakhovskiy Island. In: *Abstracts of Correlation of Pleistocene Events in the Russian North (COPERN)*, December 4–6, 2006, St. Petersburg, pp. 106–107 (in Russian).
- Tumskey, V.E., Basilyan, A.E., 2009. Quaternary stratigraphy of the Dmitry Laptev Strait coasts (Northern Yakutia). In: Kontorovich, A.E., Volkova, V.S., Khazina, I.V., Khazin, L.B. (Eds.), *Proceedings of the 6th All-Russian Quaternary Conference*. RAS SB Publishers, Novosibirsk, pp. 592–593 (in Russian).
- van Everdingen, R.O. (Ed.), 1998. *Multi-language Glossary of Permafrost and Related Ground Ice Terms*. Arctic Institute of North America, University of Calgary.
- van Geel, B., 2001. Non-pollen palynomorphs. In: Smol, J.P., Birks, H.J.B., Last, W.M. (Eds.), *Terrestrial Algal and Siliceous Indicators, Tracking Environmental Changes Using Lake Sediments*, vol. 3. Kluwer, Dordrecht, pp. 99–119.
- Vasil'chuk, Yu.K., 2006. Povtorno-zhilnye l'dy: Geterotsiklichnost', geterokhronost', geterogenost' (Syngenetic Ice Wedges: Cyclical Formation, Radiocarbon Age and Stable Isotope Records). Moscow University Press, p. 404 (in Russian).
- Vasil'chuk, Yu.K., 2013. Monograph Synopsis. In: *Syngenetic Ice Wedges: Cyclical Formation, Radiocarbon Age and Stable Isotope Records* by Yuriy K. Vasil'chuk, 2006. Moscow University Press, Moscow, ISBN 5-211-05212-9, p. 404. <http://dx.doi.org/10.1002/ppp.1764>. Permafrost and Periglacial Processes 24, 82–93.
- Vasil'chuk, Yu.K., Kim, J.-C., Vasil'chuk, A.C., 2004. AMS ^{14}C dating and stable isotope plots of Late Pleistocene ice-wedge ice. *Nucl. Instr. Methods Phys. Res. B* 223–224, 650–654. <http://dx.doi.org/10.1016/j.nimb.2004.04.120>.
- von Toll, E.V., 1895. *Wissenschaftliche Resultate der von der Kaiserlichen Akademie der Wissenschaften zur Erforschung des Janalandes und der Neusibirischen Inseln in den Jahren 1885 und 1886 ausgesandten Expedition*. Abtheilung 3. Die fossilen Eislager und ihre Beziehungen zu den Mammuthleichen. In: *Mémoires de l'Académie impériale des Sciences de St. Pétersbourg VII Série, Tome XLII No. 13*. Commissionnaires de l'Académie Impériale des Sciences, St. Pétersbourg, pp. 1–86 (in German).
- Wetterich, S., Schirmermeister, L., Pietrzniuk, E., 2005. Freshwater ostracodes in Quaternary permafrost deposits from the Siberian Arctic. *J. Paleolimnol.* 34, 363–376. <http://dx.doi.org/10.1007/s10933-005-5801-y>.
- Wetterich, S., Schirmermeister, L., Meyer, H., Viehberg, F.A., Mackensen, A., 2008a. Arctic freshwater ostracods from modern periglacial environment in the Lena River Delta (Siberian Arctic, Russia): geochemical applications for palaeoenvironmental reconstructions. *J. Paleolimnol.* 39, 427–449. <http://dx.doi.org/10.1007/s10933-007-9122-1>.

- Wetterich, S., Kuzmina, S., Andreev, A.A., Kienast, F., Meyer, H., Schirrmeister, L., Kuznetsova, T., Sierralta, M., 2008b. Palaeoenvironmental dynamics inferred from Late Quaternary permafrost deposits on Kurungnakh Island, Lena Delta, Northeast Siberia, Russia. *Quat. Sci. Rev.* 27, 1523–1540. <http://dx.doi.org/10.1016/j.quascirev.2008.04.007>.
- Wetterich, S., Schirrmeister, L., Andreev, A.A., Pudenz, M., Plessen, B., Meyer, H., Kunitsky, V.V., 2009. Eemian and Late Glacial/Holocene palaeoenvironmental records from permafrost sequences at the Dmitry Laptev Strait (NE Siberia, Russia). *Paleogeogr. Paleoclimatol. Paleoecol.* 279, 73–95. <http://dx.doi.org/10.1016/j.palaeo.2009.05.002>.
- Wetterich, S., Rudaya, N., Tumskey, V., Andreev, A.A., Opel, T., Schirrmeister, L., Meyer, H., 2011. Last Glacial Maximum records in permafrost of the East Siberian Arctic. *Quat. Sci. Rev.* 30, 3139–3151. <http://dx.doi.org/10.1016/j.quascirev.2011.07.020>.
- Winterfeld, M., Schirrmeister, L., Grigoriev, M.N., Kunitsky, V.V., Andreev, A., Murray, A., Overduin, P.P., 2011. Coastal permafrost landscape development since the Late Pleistocene in the western Laptev Sea, Siberia. *Boreas* 40, 697–713. <http://dx.doi.org/10.1111/j.1502-3885.2011.00203.x>.
- Young, K.L., Abnizova, A., 2011. Hydrologic thresholds of ponds in a polar desert wetland environment, Somerset Island, Nunavut, Canada. *Wetlands* 31, 535–549. <http://dx.doi.org/10.1007/s13157-011-0172-9>.
- Zanina, O.G., Gubin, S.V., Kuzmina, S.A., Maximovich, S.V., Lopatina, D.A., 2011. Late-Pleistocene (MIS 3-2) palaeoenvironments as recorded by sediments, palaeosols, and ground-squirrel nests at Duvanny Yar, Kolyma lowland, northeast Siberia. *Quat. Sci. Rev.* 30, 2107–2123. <http://dx.doi.org/10.1016/j.quascirev.2011.01.021>.